Physics-based Estimates of Structural Material Quantities for Urban-level Embodied Carbon Assessment in Buildings

by

Leïlah Yadia Kelly Sory

B.Eng, Civil Engineering
McGill University, 2021

Submitted to the Department of Architecture in Partial Fulfillment of the Requirements for the Degree of

MASTER OF SCIENCE IN BUILDING TECHNOLOGY

at the

Massachusetts Institute of Technology

JUNE 2023

Authored by: Leïlah Yadia Kelly Sory
Department of Architecture
May 1, 2023

Certified by: Caitlin T. Mueller
Associate Professor of Architecture
Associate Professor of Civil and Environmental Engineering
Thesis Supervisor

Certified by: Christoph Reinhart
Professor of Building Technology
Thesis Supervisor

Accepted by: Leslie K. Norford
Chair, Department Committee on Graduate Students
Professor of Building Technology

Physics-based Estimates of Structural Material Quantities for Urban-level Embodied Carbon Assessment in Buildings

by

Leïlah Yadia Kelly Sory

Submitted to the Department of Architecture
on May 1, 2023, in partial fulfillment of the
requirements for the degree of

MASTER OF SCIENCE IN BUILDING TECHNOLOGY

Abstract

Decarbonizing the built environment requires immediate actions to meet global climate targets. The world population growth and rapid urbanization rate add to the urgency of this challenge. In fact, buildings account for about 40% of all energy and carbon emissions from operations and materials' production and construction processes. More specifically, buildings' structural systems are responsible for a significant share of the upfront embodied carbon emissions before construction. Most LCA tools focus on fully detailed material takeoffs from high-resolution Building Information Models (BIM) and are therefore incomplete during conceptual design. Moreover, Urban building energy modeling (UBEM) is a proven technique allowing cities to evaluate technology pathways to achieve their net-zero emissions goals. It involves simplified building archetypes to estimate operational energy on a large scale with reasonable accuracy. However, little attention has been paid to urban-level embodied carbon assessment.

Therefore, this thesis investigates the potential of implementing physics-based structural quantities estimation in early-stage design for embodied carbon quantification at the urban scale. This approach combines bottom-up engineering calculations with data-driven surrogate modeling to automatically predict embodied carbon from a high-fidelity model. Finally, structural parameters are defined into energy model archetypes to deploy this method into an existing urban scale modeling tool. The feasibility of the proposed methodology is assessed through case studies to estimate embodied carbon and energy use intensities at the individual-building and urban scales. Results show the benefits of spatially mapping the distribution of embodied and operational carbon in the building stock and obtaining more nuanced estimates of carbon emissions compared with existing benchmarking studies. The primary use case of this work is to better inform planning and policy decision-making for retrofitting strategies and future building design.

Thesis Supervisor: Caitlin T. Mueller
Title: Associate Professor of Architecture, Associate Professor of Civil and Environmental Engineering

Thesis Supervisor: Christoph Reinhart
Title: Professor of Building Technology

Declaration

All images in this thesis are created by the author except where otherwise indicated.

Acknowledgments

I would like to express my utmost gratitude to my research supervisors, Professor Caitlin Mueller and Professor Christoph Reinhart, with whom I have been honored to work over these two years. Their guidance allowed me to forge my path and shape my research with a rigorous approach while leaving room for freedom, exploration, and curiosity. I am immensely thankful for all their advice, mentorship, and support!

My experience at MIT and within the Building Technology group has been truly unforgettable, thanks to the wonderful faculty, colleagues, and friends who have been part of my journey. I would like to thank Professor Leslie Norford, Professor John Ochsendorf, Professor Leon Glicksman, Professor Caitlin Mueller, and Professor Christoph Reinhart for creating such a positive learning environment for us. I am also thankful for our amazing administrative assistant this year, Jennifer Roesch. I have had the immense pleasure of being part of the Digital Structures Group and Sustainable Design Lab and working with the most talented and kind people I have ever met. In particular, I must thank Yiwei (Lucy) Lyu, without whom this work would not have been possible.

Throughout these two years, I have received funding through the MIT Portugal Program and travel grants from the MIT Department of Architecture that have supported my academic and professional development. Moreover, I am extremely grateful for all my collaborators from MIT Portugal, Ricardo Gomes, Joana Fernandez, Khadija Benis and Paulo Ferrão who provided me with much valuable insights and support contributing to this work.

Thank you to all of my friends, fellow students, and mentors for their encouragement.I am particularly thankful for the help I have received throughout the writing of this thesis from my writing mentor, Zuhra Faizi, and my coding mentor Cody Rose, for answering all my programming questions and teaching me so much about C-sharp.

Finally, I owe the deepest gratitude to my parents and sister. Mom, Dad, and Katia, I cannot thank you enough, and I am eternally grateful for your unconditional love and support. *Merci de toujours croire en moi et de m'accompagner dans tout ce que j'entreprends. Merci pour tout.*

Contents

List of Figures

List of Tables

Chapter 1

Introduction

1.1 Context

In the coming decades, faced with the most acute global climate crisis of human history, urgent actions have to be taken to reduce greenhouse (GHG) emissions from the built environment, which currently represent about 40% of all carbon emissions globally. The building sector is known to consume a large amount of natural resources and energy for the extraction, production, and use of construction materials. These emissions are referred to as embodied carbon. Moreover, throughout the lifecycle of a building, greenhouse emissions are also generated during the operations and maintenance of the building, which are called operational carbon (Kuittinen et al., 2023).

The world population growth and rapid urbanization rate make this challenge even more pressing. By 2050, the total world population will approach 10 billion, and by 2060 the global floor area of all building stock is projected to double (Architecture2030, 2023). In accordance with the Paris climate agreement, the world needs to halve all carbon emissions by 2030 and reach net-zero reduction targets by 2050. However, the global carbon budget for the built environment was currently estimated at 360 $GtCO_2$ (R. Weber et al., 2021).

Three scenarios are highlighted in Figure 1.1: 1) “Business-as-usual”, 2) “Net Zero Operational Carbon,” and 3) “Net Zero Operational Carbon and Embodied Carbon”. According to Weber, Mueller, and Reinhart (2021), to reach carbon emissions reduction and not exceed the remaining carbon budget of about 360 $GtCO_2$, the global renovation rate has to increase significantly from 1 to 4-5%, and decarbonization efforts need to account for both operational and embodied carbon so all new construction becomes carbon neutral by 2040.

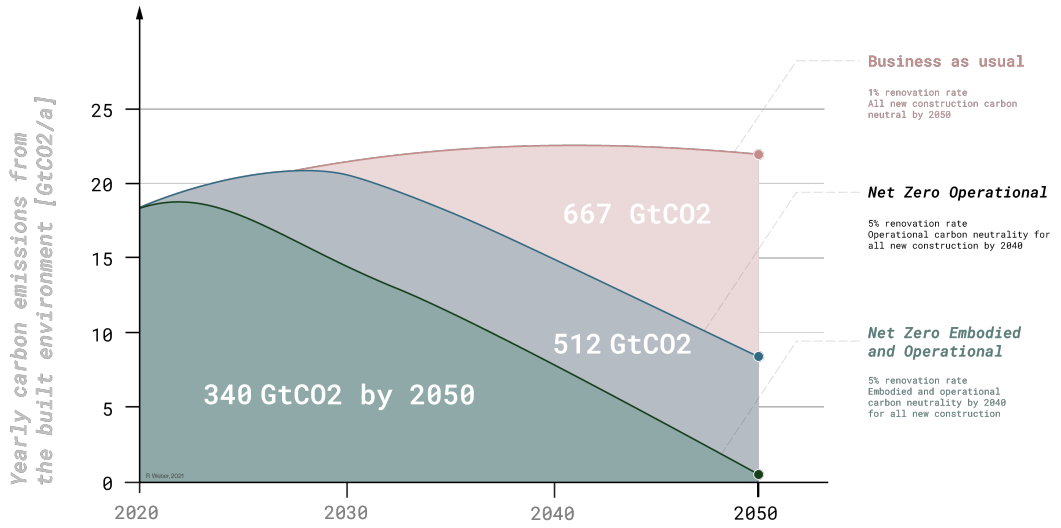

Figure 1.1: Three Scenarios of the Building for Zero Challenge (R. Weber et al., 2021).

1.2 Motivations

In the past two decades, there has been a tendency to focus on the “Net Zero Operational Carbon” path only while neglecting embodied carbon. Thus, buildings have become more and more energy-efficient while the contribution of embodied carbon to the sum total of GHG emissions over a building’s entire lifecycle keeps rising. Today, there is a growing consensus in the field that we need to urgently reduce embodied carbon along with operational carbon to achieve net-zero emissions. Therefore, reducing embodied carbon in the built environment has attracted increased interest that has led to the development of several measurement tools at the material, structural element, or whole building level using different databases and methodologies (Pomponi & Moncaster, 2018).

More importantly, reducing embodied carbon in the early design stages is a pressing challenge to tackle (Marsh et al., 2018). Given that structural material quantities represent a large portion of a building’s volume, the structural frame is recognized to have a considerable effect on lifecycle embodied emissions (D’Amico & Pomponi, 2020). Therefore, estimates of structural material quantities in early-stage design contribute to creating a valuable assessment of buildings’ embodied carbon emissions which can be refined and improved throughout the design process. Thus, informing decision-making for selecting low-carbon structural systems from the conceptual design stage (Fang et al., 2023).

However, Figure 1.2 illustrates a crucial paradox that still exists regarding the use of embodied carbon measurement tools early in the design process, as there is more design freedom, but there is also a lack of knowledge of the design variables. Therefore, the purpose of this thesis is to bridge this gap and tackle the challenges posed by the quantification of embodied carbon in buildings’ structural systems at the earliest stages of design to have the greatest potential for impact.

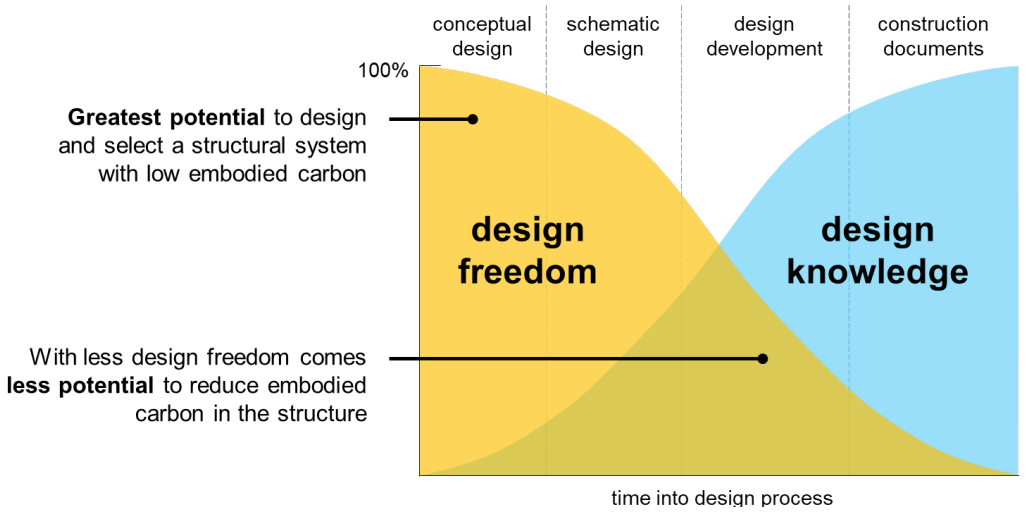

Figure 1.2: Challenges and Opportunities of Early-Stage Design (Courtesy of Caitlin Mueller and Demi Fang).

To achieve this goal, this work is focused on improving tools and methodologies for early-stage embodied carbon estimation. Figure 1.3 highlights the existing methods and tools used before a traditional fully-detailed Building Information Model (BIM) is available such as rules-of-thumb and rough estimates of structural material quantities. This thesis aims to estimate such quantities as accurately and as early as possible. Therefore, we propose a physics-based and data-driven method for an "early-stage algorithmic BIM" developed using a bottom-up approach and creating a high-fidelity structural model to allow real-time analysis in early stages when design decisions change very rapidly.

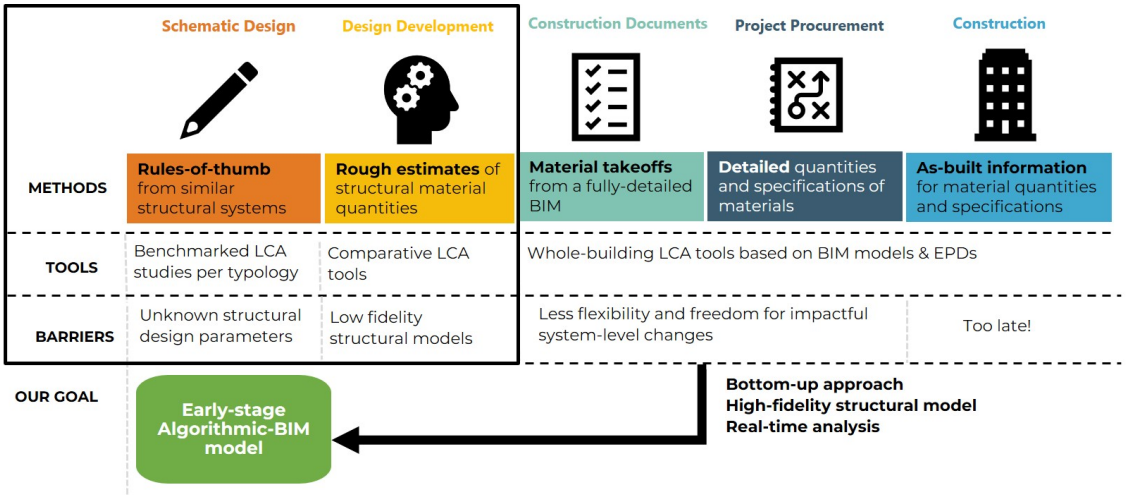

Figure 1.3: Potential to Develop an Early-Stage Algorithmic-BIM for Early-Stage Embodied Carbon Estimation.

Furthermore, this new methodology must be rapidly scaled to have a chance to decarbonize the Architecture, Engineering, and Construction (AEC) industry since urban-scale analyses have a more significant impact on achieving net zero targets. However, these studies can also be more complex, uncertain, and computationally and time-intensive.

Urban building energy modeling (UBEM) is a well-established tool that addresses these challenges and empowers cities to manage their emissions for decarbonization. For instance, successful case studies developed in collaboration with eight cities have demonstrated how policy-makers can identify technology pathways to achieve their emissions reduction goals at the building stock level (Ang et al., 2023).

1.3 Problem Statement

Different tools allow operational energy to be assessed across scales from the individual building level with Building Energy Modeling (BEM) to an urban scale using Urban Building Energy Modeling (Ali et al., 2021). However, most tools for embodied carbon emissions are focused primarily on the individual building scale using Lifecycle Assessment (LCA) and parametric models.

An LCA is an exhaustive approach requiring an inventory of the full materials used in a building (Kuittinen et al., 2023). However, building stock data required to estimate embodied carbon of buildings' structural systems is difficult to acquire, given privacy rules and the sparsity of data. Similarly, producing a parametric model requires expertise with computational tools and in this case a strong knowledge of structural design and engineering principles. Therefore, the process of creating a parametric model is challenging due to imperfections and uncertainties that can render the model unsatisfactory for use. As a result, little attention has been paid to investigating embodied carbon at the urban level.

1.4 Thesis Scope

Previous research has demonstrated that the LCA product phase A1-A3 and use phase B1-B5 are the biggest contributors to the embodied carbon of buildings (De Wolf et al., 2017). In particular, the structural system has the highest impact on embodied carbon at the product stage, while components that require maintenance and replacement have a larger impact on the use phase. Therefore, this thesis focuses primarily on the upfront embodied carbon emitted through stages A1-A3, called cradle-to-gate, while still considering the operational carbon from the use stage B6.

Moreover, since concrete and steel are by far the most used construction materials today, this thesis focuses on reinforced concrete structures. In particular, the methodology for bottom-up embodied carbon assessment applies only to the gravity system in low to mid-rise buildings, thus ignoring the contribution from the lateral system.

1.5 Research Questions

The main goal of this work is to develop a rigorous model to quantify the embodied carbon of buildings structural systems at the individual building and urban scales. Therefore, the central questions of this research are:

1) What are the key factors to consider for embodied carbon reduction in early-stage structural design?

2) How can physics-based structural quantities estimates be included for embodied carbon quantification in urban modeling?

3) How can integrated embodied and operational carbon benchmarks help cities meet their carbon reduction goals?

1.6 Thesis Structure

To answer these questions, this thesis is divided into five chapters. Moreover, the three-part methodology framework of this thesis is shown in Figure 1.4.

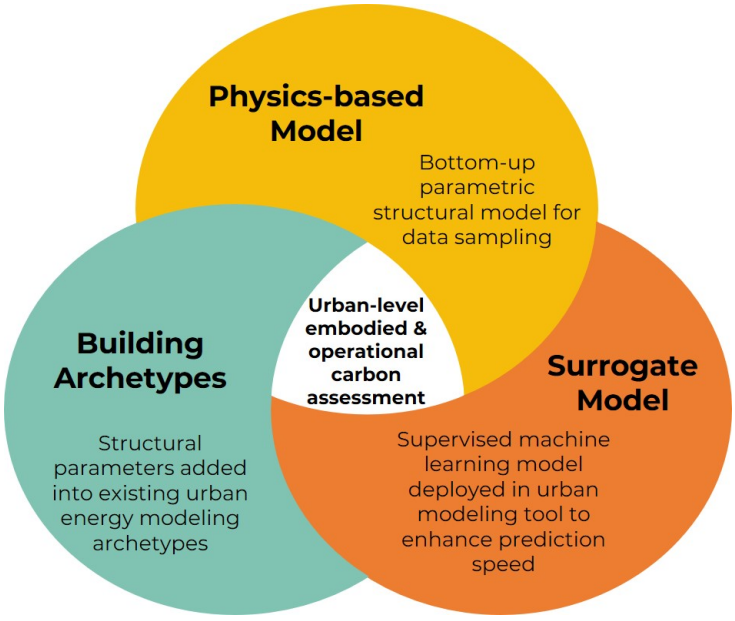

Figure 1.4: Three-Part Research Methodology Diagram.

First, a parametric model of the structural system in a multi-story reinforced concrete building is defined based on building physics to generate bottom-up calculations of structural material quantities. Second, after sampling the design space, a supervised ma-

chine learning (ML) model is trained using the acquired data with eight input features and eight outputs of structural material quantities. This model serves as a surrogate for rapidly predicting the total embodied carbon of a building structure without relying on a fully-detailed structural Finite Element Analysis (FEA). This portable ML model is then deployed within an existing urban modeling design tool for architects and engineers. Third, building archetypes are extended with the same structural parameters as the ML surrogate model and directly implemented in this tool to rapidly obtain embodied carbon results at the urban scale.

Following this introduction, Chapter 2 deals with a literature review highlighting the main research gap in urban-level embodied carbon assessment. Then, Chapter 3 covers the methodology, results, and discussions related to the physics-based and data-driven model. In Chapter 4, the methodology for deploying this portable ML model within an existing urban modeling design tool is given. Two case studies of varying scales are successfully conducted. Findings from these studies are also presented in Chapter 4 to validate this novel approach. Finally, Chapter 5 summarizes the main conclusions and contributions of this work.

Chapter 2

Literature Review

This chapter begins by reviewing the most influential body of literature describing the process for estimating and benchmarking embodied carbon at the whole-building scale with a focus on structural systems and the barriers to its implementation in early-stage design. Then, an overview of urban building energy modeling (UBEM) methods will be presented to demonstrate the application of building archetype templates for operational energy estimation.

2.1 Early-Stage Embodied Carbon Quantification

It is well known that several guidelines have been published for estimating greenhouse emissions in buildings through Life Cycle Assessments (LCAs), such as the Athena guide for whole-building LCA (Bowick et al., 2014). Moreover, several commercial and in-house LCA tools were created within the industry to measure and manage whole-lifecycle carbon emissions in buildings assessment, such as Tally, OneClickLCA, and SimaPro. However, most widely-cited reports and papers on LCA results mainly focus on measuring and benchmarking embodied carbon within detailed or as-built designs. Thus, they do not inform design decisions for early-stage embodied carbon quantification.

Fang et al. (2023) have recently analyzed the advantages, shortcomings, and state-of-the-art research of various design strategies proposed to reduce embodied carbon in structural systems as well as their compatibility with each other during early-stage design (Fang et al., 2023). In particular, three strategies directly relating to the assessment of material quantities through early-structural design were proven highly compatible with each other:

1) A prerequisite bottom-up approach,
2) A parametric design space exploration,
3) And a statistical prediction with data-driven models.

The relevance and limitations of each of these early-stage strategies are highlighted in the following sections.

2.1.1 Bottom-up Estimation of Buildings' Structures Embodied Carbon

Embodied carbon can be measured using a bottom-up approach by multiplying the structural material quantities (SMQ) of different systems with their associated embodied carbon coefficients (ECC) according to the following formula (expressed in $kgCO_2e/m^2$) (De Wolf et al., 2015):

$$GWP = \sum_{i=1}^{N} (SMQ * ECC)$$

More than 50 % of the embodied emissions in a building are contained in the structural system alone (Kaethner & Burridge, 2012). As seen in Figure 2.1, Ismail and Mueller have gauged the significant contribution of the structural system to the embodied energy (EE) of a conventional multi-story concrete building. Please note that embodied energy is directly related to embodied carbon by conversion factors. This analysis reveals that to optimize embodied carbon using a holistic approach, designers need to focus on the load-bearing structural system, which encompasses, in order of priority: horizontal slabs, foundations, as well as columns and beams (Ismail & Mueller, 2021).

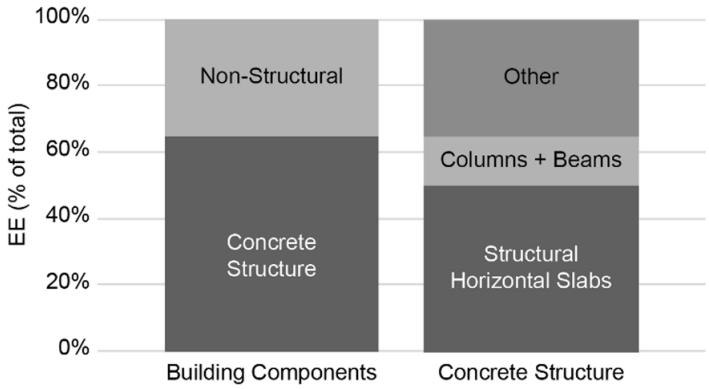

Figure 2.1: Embodied Energy of a Typical Multi-Story Reinforced Concrete Structure (Ismail & Mueller, 2021).

2.1.2 Parametric Modeling for Embodied Carbon Estimation

During conceptual design, architects and designers can use an iterative design process to assess the embodied carbon of a building. The design variables are still highly uncertain and subject to changes at this stage. By definition, measuring early-stage embodied carbon is a process with much uncertainty. Therefore, one efficient technique used to estimate embodied carbon before completing a building is through a parametric model.

A paper from Marsh, Nygaard Rasmussen, and Birgisdottir (2018) demonstrated that architects and engineers could use embodied carbon tools in early design stages by simplifying input data from the building's geometry and choosing materials and primary building elements from a database. Therefore, the outcomes of their study revealed a simplified two-step approach with a 5 to 10 % margin of error (Marsh et al., 2018). This simplification approach was deemed efficient by the authors to respond to the plethora of uncertainties in early-stage embodied carbon estimation and optimization.

Other recent studies have investigated and quantified correlations between the structural quantities of a building's gravity frame and relevant early-design choices (bay size, floor loading, and main material: either steel, concrete, or timber) to inform the comparison of different design alternatives. D'Amico and Pomponi (2020) generated and studied more than 30,000 designs using a parametric structural frame model, which outputted the amount of material normalized per floor area (D'Amico & Pomponi, 2020).

Similarly, Dunant et al. (2021) created a computational generative model satisfying specific geometric constraints to sample the design space of different design variants for comparison with the real models from a set of nineteen mid-to-low-rise designs for commercial and educational uses (Dunant et al., 2021). Through this research, the authors analyzed the influence of crucial design decisions - namely, the column layout and decking choice, on reducing steel-framed buildings' embodied carbon by almost half.

Finally, Hens, Solnosky, and Brown recently demonstrated the use of design space exploration tools to provide designers with valuable insights and visualize performance trends in the early-stage design of timber structures based on embodied carbon estimations. The authors have found that the building height and envelope area are directly proportional to embodied carbon at the whole-building level (Hens et al., 2021).

2.1.3 Surrogate Modeling of Embodied Carbon

Surrogate modeling is a common statistical approach for solving complex engineering problems more efficiently based on a predictive model. This is possible because the statistical regression model is capable of making fast predictions after learning patterns and relationships from some input and output data. This process is part of the branch of machine learning called supervised learning.

In sustainable design, surrogate models have been used for rapidly predicting and analyzing the performance of a building, especially when conducting conceptual design, sensitivity analysis, uncertainty analysis, and optimization (Westermann and Evins, 2019). Recently, surrogate modeling has also been applied to estimate embodied carbon in buildings. Since performing a Finite Element Analysis (FEA) of a structural model is time and computationally intensive, a surrogate model has the benefit of enhancing the prediction speed and facilitating predictions on a large scale.

Data-driven models used for this purpose have been obtained in two ways: 1) using historical data, or 2) using synthetic data generated through a parametric workflow, for instance. Victoria and Perera created a parametric model and developed a regression model of embodied carbon prediction using historical data of office buildings of low to medium-rise in the United Kingdom (Victoria & Perera, 2018).

Furthermore, surrogate models can use several types of algorithms: Random Forest, Kernell Ridge Regression, and Neural Network, to cite a few. Tseranidis, Brown, and Mueller (2016) demonstrated a validation approach with the comparison of these six surrogate modeling algorithms by evaluating each model's performance and selecting the best model to quickly explore and optimize the design space of civil structures (Figure 2.2) (Tseranidis et al., 2016).

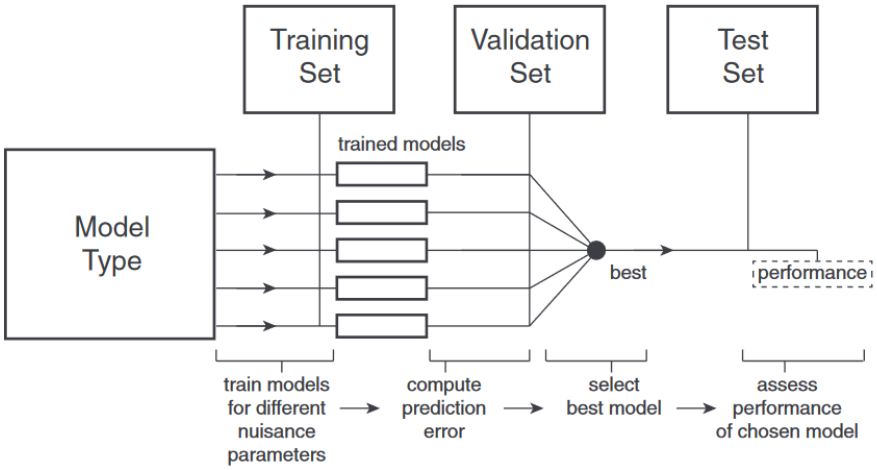

Figure 2.2: Application of Surrogate Modeling in Design (Tseranidis et al., 2016).

Similarly, in a more recent study, Pomponi et al. (2021) compared the performance of different surrogate models and used three types of materials: reinforced concrete, steel, and timber, to predict the amount of material and embodied carbon contained in the structural systems (Pomponi et al., 2021).

2.2 Context on Embodied Carbon Benchmarking

While designers have the greatest potential to reduce embodied carbon in buildings' structures early in the design process, they are also limited by the lack of global, reliable, and comparable benchmarks - mainly due to uncertainties in datasets and methodologies.

2.2.1 Research Efforts: Databases and Methodologies

Databases of Environmental Product Declarations (EPDs) and building data such as the Embodied Carbon in Construction Calculator (EC3) database provide pertinent information to improve embodied carbon estimation in the industry at a national and even global scale (De Wolf et al., 2017). Since 2017, the work of Simonen, Rodriguez, and De Wolf has allowed to establish a uniform database of embodied carbon at the whole building level with reliable benchmarks. The authors created an Embodied Carbon Benchmark (ECB) Study to address some questions about the order of magnitude and variation of embodied carbon, the sources of uncertainty, and different benchmarking strategies (Simonen et al., 2017). Figure 2.3 reveals the ranges of the initial embodied carbon assessed in different building types from this database.

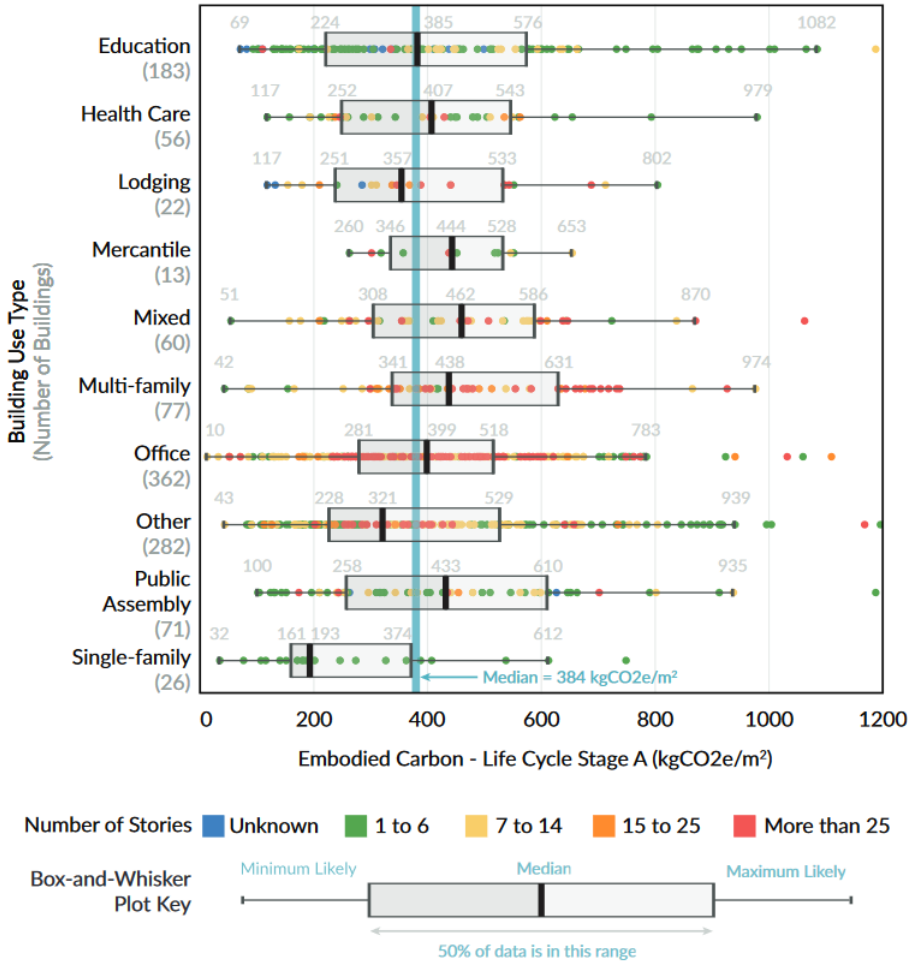

Figure 2.3: Embodied Carbon Benchmark Study (Simonen et al., 2017).

The ECB Database is composed of more than 1000 buildings provided by different architecture and engineering firms such as Arup, SOM, and Thornton Tomassetti, and research databases such as WRAP and DeQo developed at MIT.

2.2.2 Challenges and Barriers to Implementation

Despite these efforts, the AEC industry and researchers have not yet managed to agree on a systematic approach to benchmark embodied carbon. Therefore, embodied carbon is still at the heart of a “second wave” of the performance gap in buildings’ environmental assessment. Pomponi and Moncaster have investigated in more detail the data and methodologies used in embodied carbon assessments to understand the limitations of their applications. Their work revealed some explanations for the gap between calculated and actual embodied carbon measurements, such as data scarcity and variability (Pomponi & Moncaster, 2018). Similarly, De Wolf, Pomponi, and Moncaster (2017) identified barriers and drivers to the applications of embodied carbon measurement in practice.

2.2.3 Opportunities: Tools for Integrated Embodied and Operational Carbon Assessment

Promising tools automatically generate a structural model and allow the comparison of different design alternatives by rapidly assessing embodied and operational carbon in the early design process. In a recent study, Weber, Mueller, and Reinhart have developed a physics-based method to measure embodied carbon from existing buildings’ structural systems using a generative algorithm. This new method proposes to calculate the structural quantities and embodied carbon of a steel framing system with a sub-17 % error margin and can be applied at the urban scale (R. E. Weber et al., 2021).

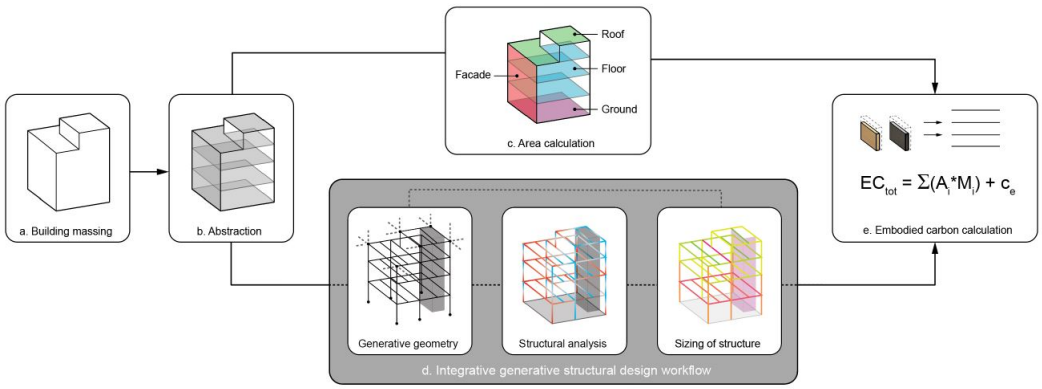

Figure 2.4: Generative Embodied Carbon Model Workflow (R. E. Weber et al., 2021).

Architectural, structural, and energy models have their own set of geometric and non-geometric parameters and requirements used to assess the building's performance. However, these models are complementary and can build upon each other when combined to improve the accuracy of their associated simulations.

In 2021, Kral suggested a new algorithm called AutoFrame to convert any architectural massing into separate structural and energy models to simulate building performance and assess lifecycle carbon emissions (from embodied to operational) at early stages (Kral, 2021). This new approach aims to integrate the existing energy and daylight simulation tools with a robust structural model approximation for estimating material quantities and embodied carbon of a framed building made of timber, concrete, or steel. Thus, allowing for a dynamic and multi-dimensional environmental performance assessment from the onset of the conceptual design process when there is a greater potential for impact. AutoFrame results in a 0.5 to 12.5% error margin in embodied carbon estimation for designs with refined inputs and up to 33.5% for those defined with coarser inputs.

Furthermore, a sensitivity study of various design parameters of typical residential and office multi-story buildings was recently published to analyze their effects on embodied carbon, construction costs, and heating and cooling loads. These parameters included: the building's shape, size, typology, layout, and structural system (Gauch et al., 2023). Gauch et al. demonstrated that embodied and operational carbon are most sensitive to the building size and shape, along with the structural system type and layout, which are decisions taken at the early stages of design. There is also a tradeoff between embodied and operational carbon based on the number of stories. The higher the number of stories, the higher the embodied carbon and the lower the operational carbon. This is because structural material quantities will increase with more stories.

2.3 Urban Building Energy Modeling and Building Archetypes

2.3.1 State-of-the-art

Urban Building Energy Models (UBEMs) allow designers, urban planners, and cities to determine or predict the operational energy consumption of an existing or new urban building stock. Two types of UBEMs exist 1) top-down models and 2) bottom-up models. Figure 2.5 summarizes the strengths and limitations of each model.

The top-down approach relies on aggregated historical data on energy use and techno-socioeconomic factors on a macro scale to make long-term energy use predictions. In contrast, the bottom-up approach is more effective for detailed urban building modeling as it uses a disaggregated approach considering individual buildings or groups of buildings with simplified building templates called archetypes (Abbasabadi & Ashayeri, 2019) (Ali et al., 2021).

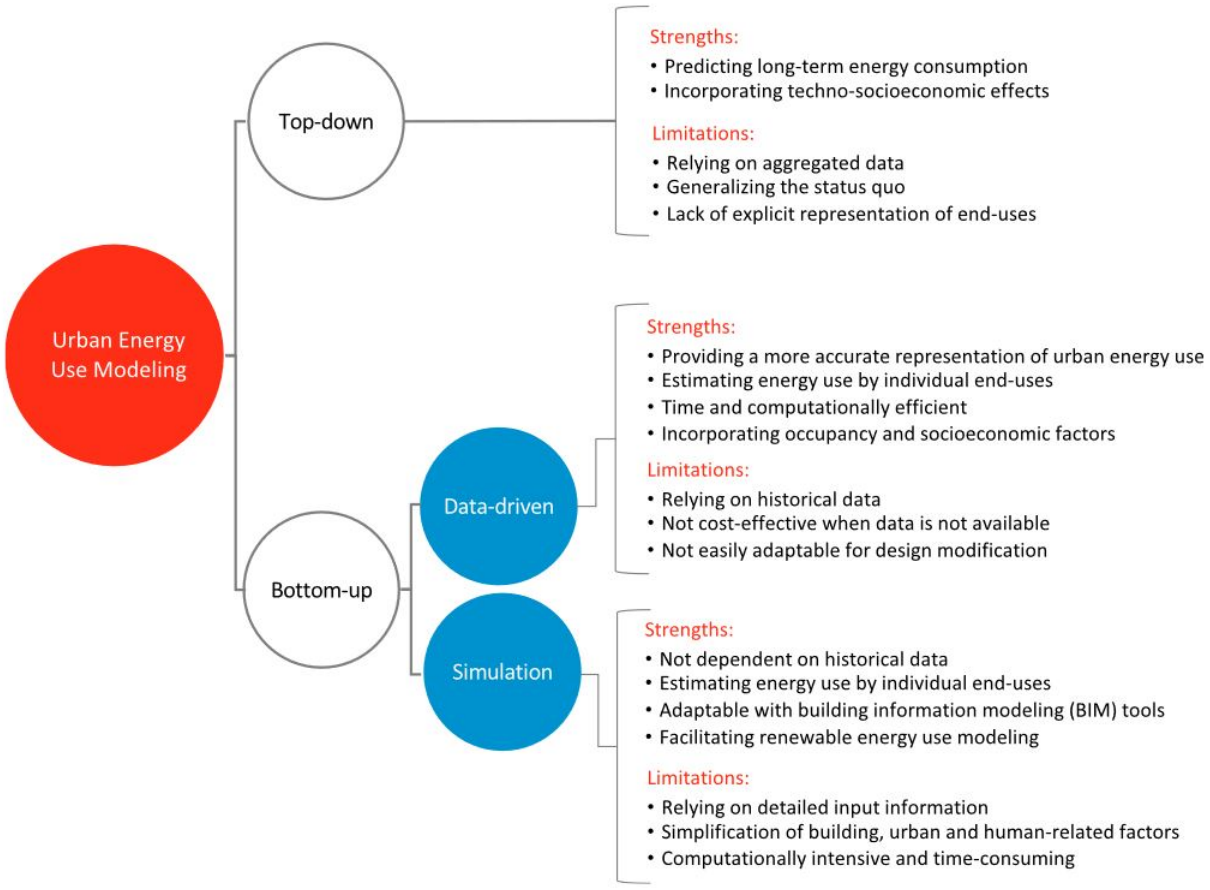

Figure 2.5: Strengths and Limitations of Top-down and Bottom-up Urban Energy Use Modeling Approaches (Abbasabadi & Ashayeri, 2019).

Among bottom-up approaches, statistical-based or data-driven models use historical data on relevant building characteristics from GIS data and surveyed data such as energy use, occupancy, and other socioeconomic factors. On the other hand, simulation models use a physics-based approach and require a granular level of buildings' geometric and non-geometric input information defined in building archetypes. It is important to calibrate the results obtained from physics-based models using real measured data since building archetypes only provide a simplified picture that is not representative of the actual diversity of specific buildings and can be seen as arbitrary and subjective. Therefore, creating physics-based models can be a particularly long and computationally-intensive process (Ali et al., 2021).

Both data-driven and physics-based techniques have limitations in creating realistic UBEMs due to the uncertainties in methodologies, the complexity of urban systems, the lack of data availability on a large scale, and the significant computational needs of urban modeling (Abbasabadi & Ashayeri, 2019). However, this thesis is focused on the bottom-up physics-based method, which is currently the most prevalent in urban modeling.

2.3.2 Building Archetypes for Urban Scale Energy Modeling

To perform a physics-based urban scale simulation, a seed model of a city, specific neighborhood, or site is first defined. This model covers a limited area composed of airtight 3D building massings obtained from GIS data and involves only planar surfaces and context objects such as shading, site boundary, and streets. Each massing holds the geometric information, complemented by a building archetype including site, climate information, and important non-geometric parameters (Cerezo Davila, 2017).

Building archetypes are defined by segmenting the available building stock data based on similar shared attributes such as vintage and program. Following this, each archetype is characterized depending on specific building attributes such as construction assemblies and materials. Finally, the archetypes are assigned to the building stock creating a spatial distribution of buildings' templates and quantifying the number of buildings for each archetype. It is essential to define reliable archetypes to avoid garbage-in and garbage-out simulations and unacceptable inaccuracies in simulation results (Cerezo Davila, 2017).

The Urban Modeling Interface (UMI) is a tool implemented in the architectural design software, Rhinoceros3D. Developed by the MIT Sustainable Design Lab, this simulation tool incorporates six modules enabling designers to efficiently conduct a comprehensive, multi-dimensional urban-scale analysis for their projects and visualize the results to guide their decisions: site analysis, operational energy, lifecycle, district energy, urban agriculture, and design accessibility. Figure 2.6 shows the UMI User Interface and its various modules.

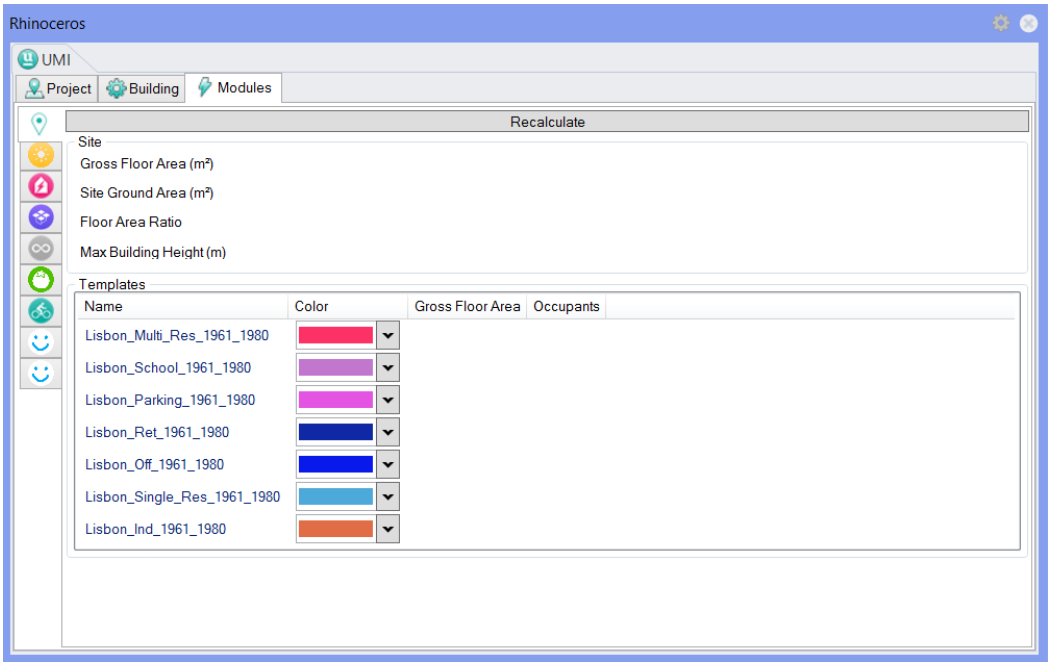

Figure 2.6: UMI User Interface.

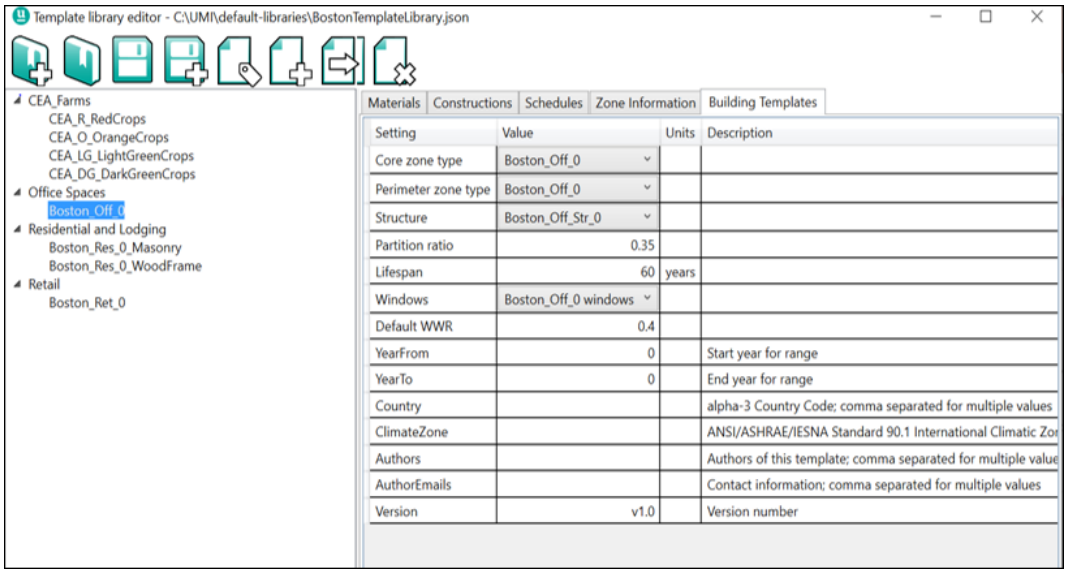

Figure 2.7: UMI Building Template Library Structure.

Within UMI, building archetypes are stored in a template Library in the form of XML files holding the information required for urban modeling. A Template Editor was created as a UMI-supporting application, allowing users to manage their templates by directly populating various template-specific settings for their projects. An extensive library of templates has already been established for operational models, including zone information from internal loads to conditioning systems, energy use schedules, and construction assemblies, as shown in Figure 2.7. Before running each urban simulation, it is important to collect enough information to have a good representation of the building archetypes and populate them using the Template Editor.

In the current version of the Lifecycle module in UMI, opaque construction assemblies are defined by their composing materials and thicknesses to allow the bottom-up estimation of embodied carbon in the following five construction systems: 'Facade,' 'Ground,' 'Partition,' 'Roof,' and 'Slab,' as well as 'Windows.' In addition, an assumption is made to consider a constant area normalized ratio for the structure in a specific building template. Based on this rule of thumb, the structural material quantity is then multiplied by the embodied carbon coefficient of the associated material to determine a zeroth-order approximation of embodied carbon. Accordingly, this estimation is overly-coarse and does not provide the designers the flexibility to reduce the embodied carbon of the structural system effectively.

2.3.3 Case Studies on Urban-Level Embodied Carbon Assessment

Most of the applications and benchmarking efforts of UBEMs conducted in the past have focused only on operational energy. However, two types of embodied carbon assessment

at the urban level have started to emerge: 1) benchmark analysis with surveyed data and 2) spatial analysis with maps of carbon hotspots.

An extensive benchmarking report was recently published using data assembled from five European countries to provide harmonized embodied carbon benchmarks for buildings in Europe (Röck et al., 2022). Figure 2.8 presents the breakdown of embodied carbon intensities for different building parts: Ground, Structure, Envelope, Internal, Services and Appliances. However, the lack of available data and uncertainties in methodologies make the process of defining these benchmarks particularly challenging.

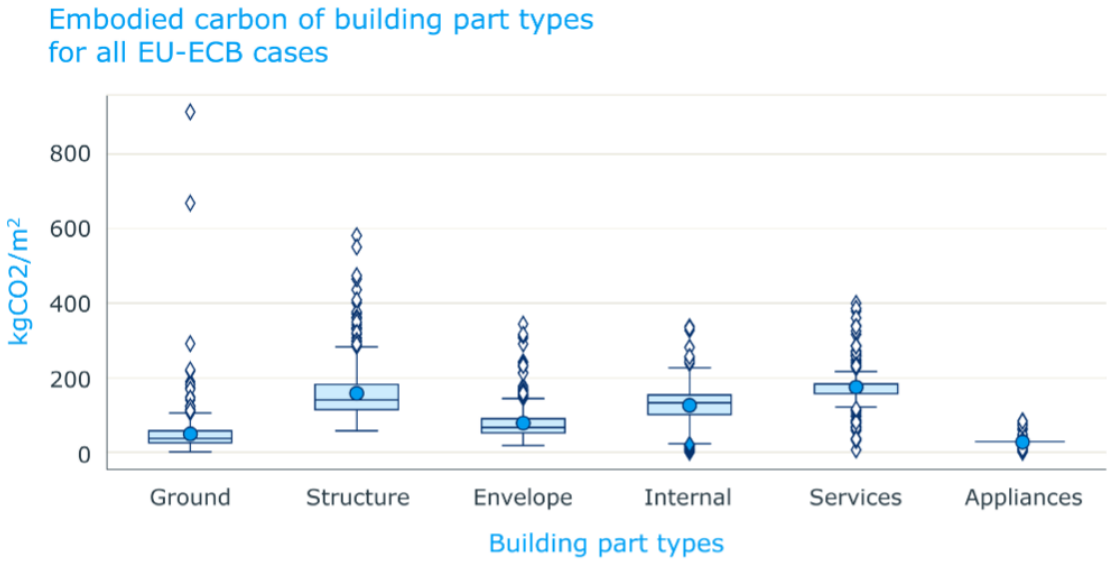

Figure 2.8: EU Benchmark Study Breakdown (Röck et al., 2022).

Furthermore, an example of a bottom-up spatial analysis that quantifies embodied environmental impacts was conducted at the city level to model the building stock in Melbourne, Australia (Stephan & Athanassiadis, 2017). This work demonstrates the importance of quantifying the emissions that could result from rebuilding a city's stock today and highlights the spatial distribution of carbon hotspots. Hence, providing insights to cities to better manage their building stock and meet their carbon reduction goals.

This literature review highlights the critical knowledge gap and opportunity concerning the estimation of structural material quantities for embodied carbon assessment in urban modeling, which is a major contribution of this thesis.

Chapter 3

Physics-Based and Data-Driven Model for Early-Stage Structural Sizing

This chapter describes the first part of the research methodology designed to develop a physics-based and data-driven surrogate model and analyzes the results obtained from this early-stage structural quantities estimation.

3.1 Methodology for Generating a Parametric Structural Model

As mentioned in the previous chapter, using a parametric model is one of the most efficient techniques for performing a bottom-up estimation of embodied carbon in the early design stages. In this study, the full-building parametric model (Figure 3.1) was created using Grasshopper - a visual programming environment associated with the 3D modeling software Rhinoceros3D.

Following conventional construction practices in the concrete sector, the model is based on a typical reinforced concrete frame with a rectangular grid and comprises three major structural systems: 1) the structural frame and 2) the slab system, which constitute the superstructure, and 3) the foundations, which represent the substructure. In particular, the frame is composed of columns as vertical components and primary and secondary beams contributing as horizontal members.

3.1.1 Structural Assumptions and Limitations

The parametric model includes specific ranges of eight input parameters related to the building geometry, typology, materials, and soil conditions, as represented in Table 3.1.

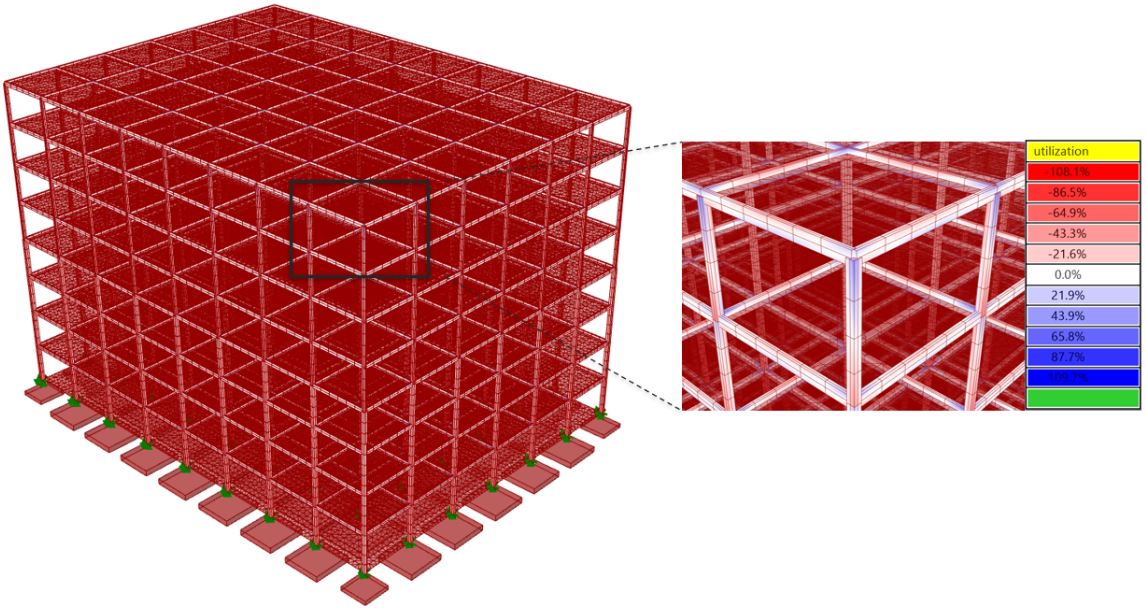

Figure 3.1: Structural Model.

Table 3.1: Model Input Parameters and Constraints.

Model inputs	**Range**	**Units**
Floor-to-floor height	2.5-5	m
Number of stories	2-10	
Primary span	3-12	m
Secondary span	3-12	m
Program and live load	Residential: 1.92 Office: 2.40 Hospital: 2.87 Assembly: 4.79 Retail, Warehouse: 6	kPa
Concrete strength (slabs, beams, foundations)	17.3-55.1	MPa
Concrete strength (columns)	17.3-55.1	MPa
Soil type and soil bearing capacity	Clay: 72 Sand: 97 Gravel: 144	kPa

It is worth noting that the building model is designed to resist gravity loads and does not yet include a lateral bracing system. As a result, the number of stories in the model is limited to 10, a point up to which a building can reasonably rely on the gravity system only (D'Amico & Pomponi, 2020). The primary and secondary spans which define the column grid have typical ranges for non-prestressed reinforced concrete, as longer spans would

require some post-tensioning to be included. As for building typology, the live loading of the following six chosen programs was obtained in Table 4.3-1 from the ASCE/SEI 7-22 Standard by the American Society of Civil Engineers: residential, office, hospital, assembly and retail or warehouse. Moreover, two types of concrete with compressive strength ranging between 2,500 and 8,000 psi (equivalent to 17.3 and 55.1 MPa) were selected for the slabs, beams, and foundations on the one hand and the columns on the other. Given that the parametric model represents low-to-mid-rise buildings, the three most common types of soil conditions encountered with shallow foundations were considered: clay, sand, and gravel.

Table 3.2: Model Material Properties Assumptions.

Material	**Design Strength [MPa]**	**Modulus of Elasticity [MPa]**	**Embodied carbon coefficients [$kgCO_2/m^3$]**	**Embodied carbon coefficients [$kgCO_2/kg$]**
Concrete	17.3	21,029	240	0.100
	20.7	23,002	262	0.109
	27.6	26,561	308	0.128
	34.5	29,696	365	0.152
	41.3	32,491	385	0.161
	55.1	37,528	446	0.186
Steel	415	205000000	16,020	1.99

Some assumptions are also made about the reinforced concrete's mechanical properties for the structural analysis and can be found in Table 3.2. The parametric model is built assuming a typical normal-weight concrete with a density of 2400 kg/m^3. The embodied carbon coefficients of concrete are obtained from a recently published cradle-to-gate LCA report prepared for the National Ready-Mixed Concrete Association (NRMCA) by the Athena Sustainable Materials Institute based on national industry average data from the United States (Athena Sustainable Materials Institute, 2022). As for the steel reinforcement, standard properties from ASTM 50 steel rebars are chosen with a density of 8050 kg/m^3. Finally, an established value of 1.99 $kgCO_2e/kg$ is taken for the embodied carbon coefficient of the steel rebar following the ICE database (ICE, 2019).

3.1.2 Structural Model Analysis

One of the key contributions of this thesis is the creation of a parametric workflow for the structural design of a whole-building reinforced concrete model[1]. An overview of the parametric model workflow is presented in Figure 3.2, which shows the set of constraints and checks required in the iterative design process. At the start of this workflow, the floor and roof slabs are designed according to engineering first principles and the ACI 318-19(22): Building Code Requirements for Structural Concrete. Then, the structural analysis of the frame elements can be carried out using the Grasshopper plug-in Karamba3D

[1]The model was designed through a collaborative effort with Yiwei Lyu and Kiley Feickert.

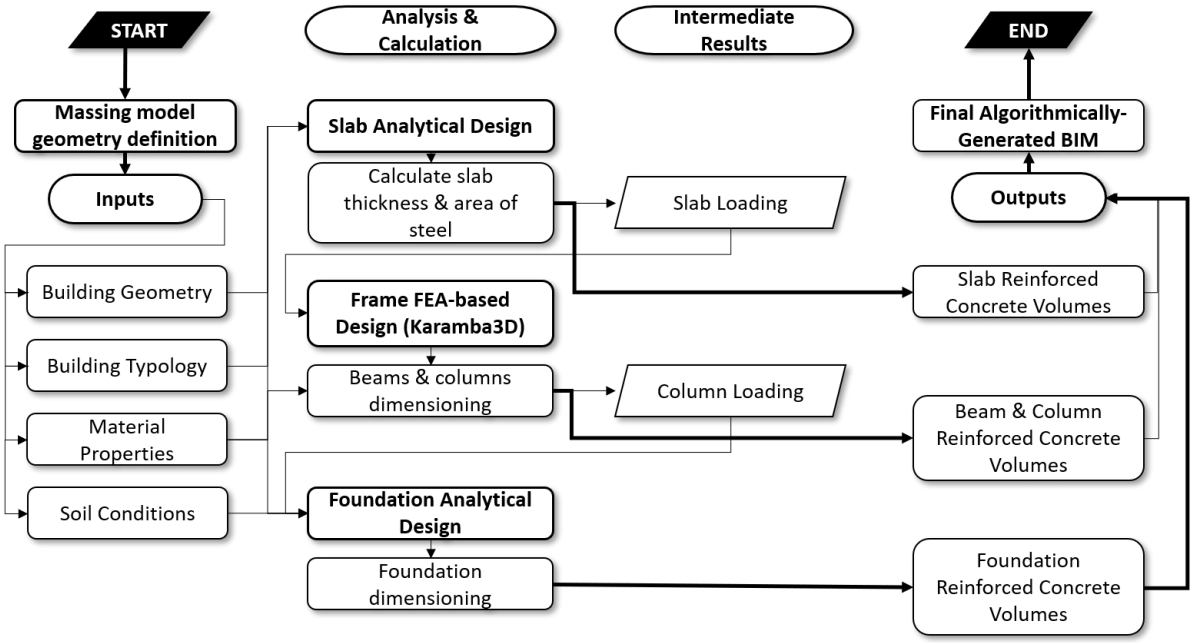

Figure 3.2: Parametric Workflow for Structural Model.

by evaluating the structural performance of each component through streamlined Finite Element Analyses (FEA). Finally, the design of the spread foundations is derived from analytical relationships involving soil-bearing capacity and column loads established by Feickert (Feickert, 2022).

Based on the sizing of each structural system, the parametric model yields eight outputs for the volumetric quantities of concrete and steel material across the slabs, beams, columns, and foundations. The following sub-sections will further discuss the design of each structural system: 1) slab design, 2) frame design, and 3) foundation design.

Slab Design

As a non-prestressed concrete two-way slab system, the current model assumes that the floor system is simply-supported on all four sides by beams, thus neglecting the effect of torsion at the edges. Therefore, based on the Rankine-Grashoff's approximate strip method, the moment demand of the slab is calculated in the short and long directions using the following equations:

$$Mu_x = \beta_x w l_x^2 \ , \ Mu_{\text{y}} = \beta_y w l_y^2 \tag{3.1}$$

Where the coefficients $\beta_x = \frac{\alpha^4}{8(1+\alpha^4)}$ and $\beta_y = \frac{\alpha^2}{8(1+\alpha^4)}$ were calculated using the aspect ratio, $\alpha = \frac{l_y}{l_x}$

It can be noted that these analytical equations are also valid when designing a one-way slab system, given that the moment coefficients β_x and β_y reflect how the load is propor-

tionately distributed in both directions. Hence, for one-way slab systems, most of the load will be transferred to the shorter span. Because this parametric model assumes that the slab is supported by beams on all four sides, in the case of a one-way system, the dimensions of the secondary beams are reduced and yield much thinner cross-sections than that of the primary beams. For the slab design, both the concrete cover and the diameter of the steel reinforcement bars are fixed at specific values of 40 mm and 25 mm, respectively. It is also important to note that a minimum slab thickness is initially assumed according to equation (2) taken from a code-based rule-of-thumb accounting for deflection control:

$$d = \frac{l_x}{33} \tag{3.2}$$

In addition to calculating the moment demand, the design workflow includes additional steps to check the shear demand of the slab. In the calculation for shear capacity , v_n, only the concrete is assumed to contribute as v_c, ignoring the steel reinforcement contribution. Hence, the shear capacity is obtained as follows:

$$v_n = (v_c + 0.66 f_c^2 b_w d) * 10^3 \tag{3.3}$$

Similarly, the shear demand, v_u, based on the tributary area is found to be:

$$v_u = w(0.5 l_x - 0.5 b_w - d) \tag{3.4}$$

Where f_c represents the concrete strength, and b_w and d are the slab cross-section width and effective depth.

The slab dead load includes its self-weight and a superimposed non-structural dead load value of 1.0 kPA. Two load cases were considered to be dominant for our model of the gravity system, which does not include wind, snow, and earthquake loads: 1) 1.4*Dead Load and 2) 1.2*Dead Load + 1.6*Live Load.

The required slab thickness is then iteratively increased to satisfy the shear check loop and considering deflection control. Finally, the moment demand, M_u is used to obtain the required area of the reinforcing steel based on rule-of-thumb calculations. The equations used are detailed as follows and involve a constant derived in metric units by Ismail and Mueller (Ismail & Mueller, 2021):

$$A_s = \frac{M_u * 10^6}{constant * d}$$

$$constant = 0.87 * f_y * (1 - 1.005 * \rho * \frac{f_y}{f_c}) * 10^{-3}$$

$$\rho = \frac{2}{3} * (\frac{0.36 * f_c}{0.87 * f_y}) * (\frac{\epsilon_c}{\epsilon_s + \epsilon_c})$$

Where ϵ_c represents the concrete strain, and f_y and ϵ_s, the steel strength and strain.

Frame Design

The structural analysis of the columns and beams is performed with the parametric structural design tool, Karamba3D. As mentioned previously, the model focuses on gravity load design and ignores lateral loads. A homogeneous reinforced concrete material is created for the frame design, assuming that all of the tensile strength of the material is provided by the reinforcing steel and thus equals the compressive strength of the concrete. Consequently, an assumption of 2% of reinforcing steel volume was applied to separate the volume contribution from the concrete and the steel for the columns and beams.

The beams and columns cross-sections are optimized to withstand the loading transferred from the slabs. The beams are given rectangular cross-sections and constrained by a maximum height of 1m. Moreover, because the geometries of the beams and slabs were initially overlapping in the model, the additional volume of the beams is removed from the slabs' volume. Columns are assumed to have a squared cross-section and not rectangular as beams since potential buckling effects are not accounted for in the design. Furthermore, the cross-sections of the columns are allowed to change when the number of stories exceeds five such that the group of upper columns can take smaller cross-sections than the group of lower ones. This method is equivalent to changing the reinforced concrete strength of the columns based on the number of stories - for example, by reducing the area of the reinforcing steel. This is a common construction practice since columns on upper floors carry fewer loads and can use lower-strength concrete mixes.

Foundation Design

The foundation design follows a workflow developed by Feickert (2022) to size the dimensions of spread and shell footings depending on the soil-bearing capacities and column loads. Therefore, this workflow defines the volume of concrete and steel in the foundation system and its resulting embodied carbon. Because of the parametric model's limitation for low- to mid-rise buildings only spread footings and the three most common soil types with lower bearing capacities are considered: clay, sand, and gravel.

3.1.3 Design Space Sampling and Data Processing

The physics-based model algorithmically generates a simplified BIM, which outputs the volumetric quantities of concrete and steel within each structural system in units of kg/m^3. Synthetic data from the parametric model can be randomly generated and sampled at a significantly fast rate of about 5 minutes for 100 designs, or about 3 seconds per design. A large dataset of 130,000 data was collected. The reason why the parametric model generates structural quantities and not embodied carbon estimates is to facilitate future updates to the dataset using more accurate embodied carbon coefficients.

Next, the data processing step consisted of calculating each structural system's embodied carbon from their material quantities with the help of associated embodied carbon coefficients. The structural material quantities and embodied carbon values were also

normalized per floor area, allowing for better comparisons across different designs. Another crucial part of the data processing step was to scale all input features and outputs to obtain a mean of 0 and a standard deviation of 1.

After sampling the design space and preparing the dataset, a supervised machine learning (ML) model was trained using the acquired data with eight input features and eight outputs of structural material quantities.

3.2 Methodology for Building a Neural Network Surrogate Model

3.2.1 Model Training and Hyperparameters Tuning

The neural network model[2] is built using a typical Multi-Layer Perceptron (MLP) architecture from the Pytorch library environment and learns on the dataset of 130,000 samples acquired from the parametric model with a validation dataset size of 20% and 80% for the training data. This Neural Network is based on a feed-forward model, which includes an input layer, 14 hidden layers, and an output layer, as shown in Figure 3.3. The activation function and optimizer were chosen to be ReLu and Adam, respectively, as is usually recommended for neural network model training. The following list provides the number of hidden neurons within each hidden layer which was chosen intuitively and proven effective during training: [128, 128, 128, 128, 128, 512, 512, 512, 512, 128, 128, 128, 128, 128]. The loss function used during model training is the mean squared error (MSE) which is particularly common in machine learning and data science applications.

Additionally, three model hyperparameters were systematically tuned in a non-exhaustive search to determine the best combination of hyperparameters for the batch size, the number of epochs, and the learning rate.

3.2.2 Evaluating Surrogate Model Performance

After training nine neural network models by varying their hyperparameters, the training and validation sets were used to calculate their associated MSE loss. The best surrogate model displaying no signs of overfitting was then selected. This means that the model's testing loss was the lowest and did not start increasing at some point, while the training loss kept decreasing. Indeed, overfitting occurs when the model fits the training data extremely well and, consequently, cannot generalize to any other dataset. Furthermore, it was essential to assess the model performance by determining its generalization error on a new unseen testing dataset which was different from the training and validation sets. This error allows to characterize the difference between the actual values and the model predictions to determine whether the model generalization error is acceptable.

[2]The model was designed in collaboration with Yiwei Lyu.

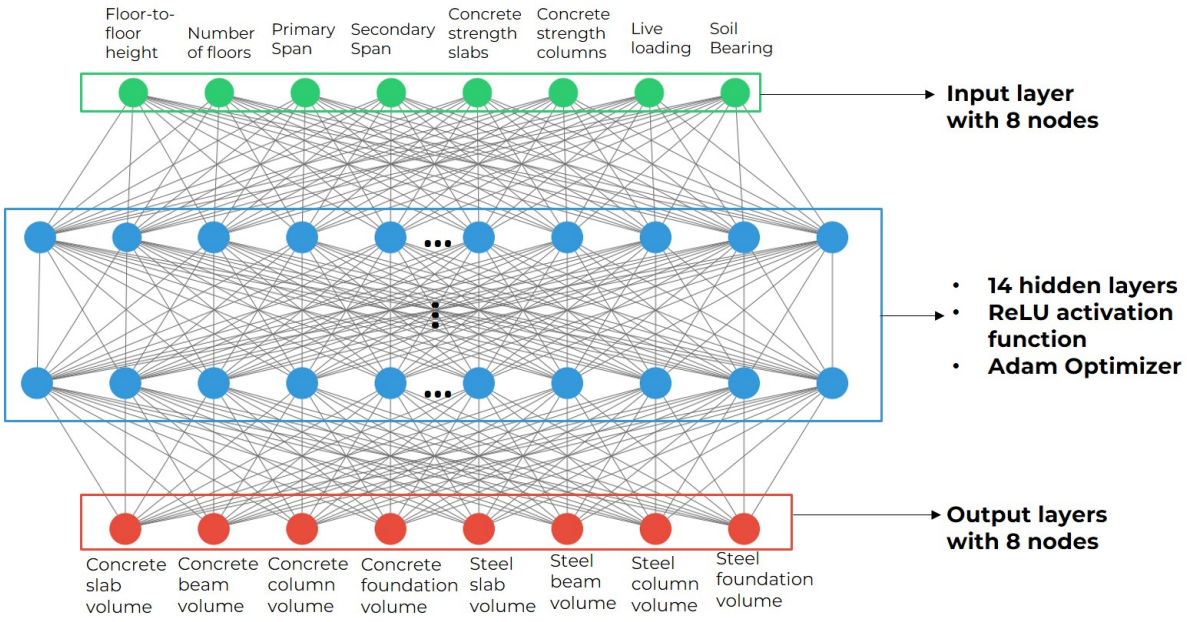

Figure 3.3: Feed-forward Neural Network Architecture Representation.

3.3 Results and Discussion

3.3.1 Exploratory Data Analysis

Before using the processed dataset to build the surrogate model, an exploratory data analysis was conducted to inspect all 100,000 training data samples. Therefore, different visualization tools were used to explore trends or patterns in the data.

Figure 3.4 shows a histogram of the total normalized embodied carbon distribution and highlights the 10th and 90th percentiles to identify designs with the lowest and highest embodied carbon values. Values below the 10th percentile are coloured in green; values above the 90th percentile are shown in yellow while any value in between is shown in blue. Even though this frequency graph seems to lean towards a normal distribution, it appears slightly skewed to the left, with a smaller noticeable peak below the 10th percentile. This observation can be explained due to the assumptions made in the parametric model design. Indeed, the slab design process includes a minimum thickness as shown in Equation 3.2. Because of this structural code requirement, the minimum slab thickness can be chosen more regularly, which leads to this second peak for lowest-embodied carbon designs.

In addition, four stacked bar charts in Figure 3.5 display the contribution of concrete and steel reinforcement to the embodied carbon within each structural system and for each building typology defined previously in Table 3.1.

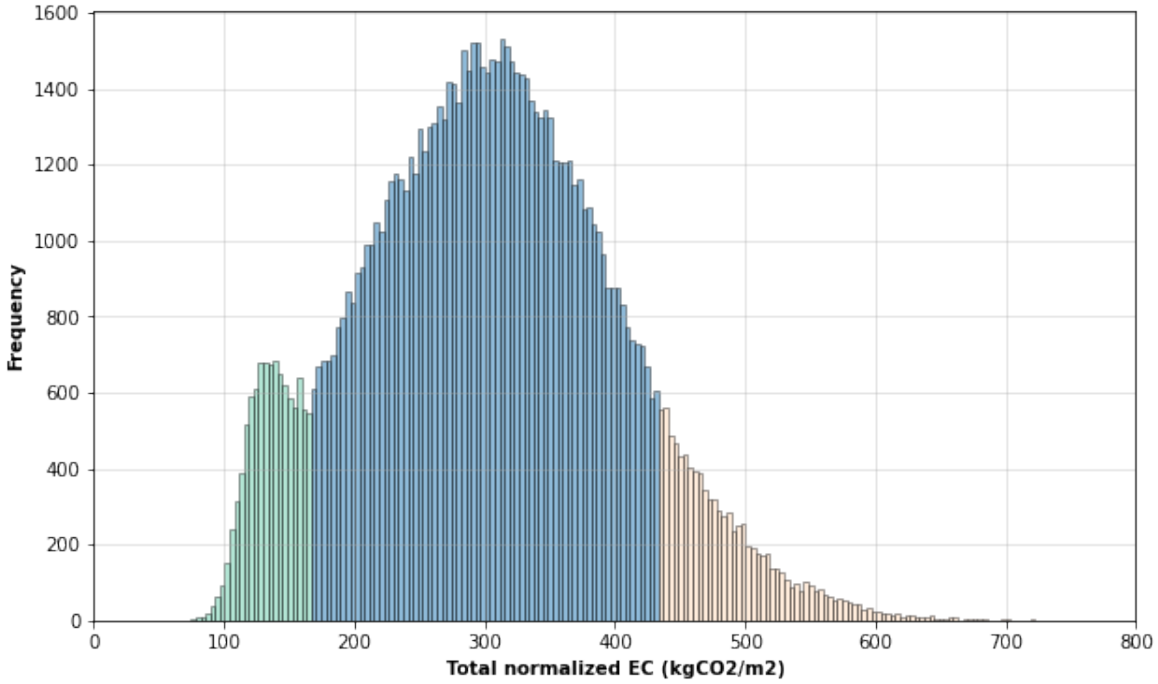

Figure 3.4: Total Normalized Embodied Carbon Distribution.

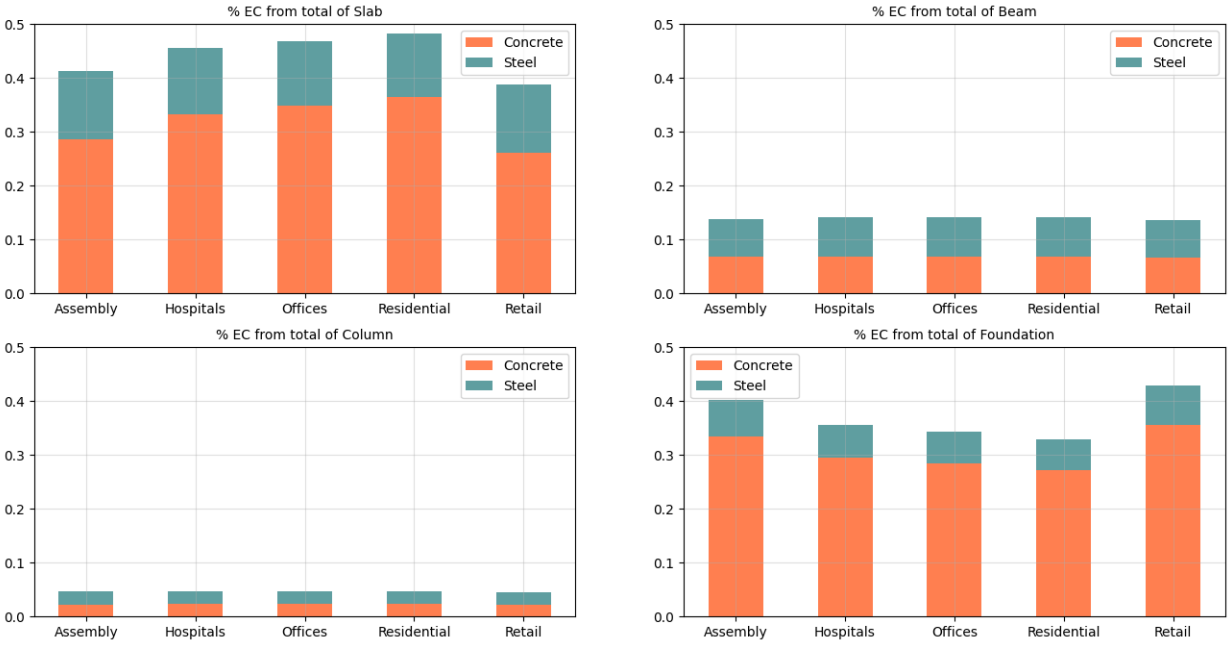

Figure 3.5: Contributions of Concrete and Reinforcing Steel to Total Embodied Carbon Across Different Building Types and Parts of Structural Systems.

The contribution from steel and concrete appears to be about the same (50% each) for beams and columns; however, for slabs and foundations, the concrete clearly dominates (by at least 75 %). Surprisingly, the contribution of steel reinforcement to embodied carbon largely exceeds the volumetric ratio used in the structural analysis of these systems. For example, only 2% of steel reinforcement is assumed in the frame analysis. This is because the embodied carbon coefficient of steel is more than ten times higher than that of concrete as seen from Table 3.2. Hence, this graph highlights that steel is an important contributor to a reinforced concrete building's embodied carbon. Regarding the comparison between typologies, it can be noted that the higher the live load (Assembly and Retail), the lower the contribution of the concrete within the slabs is to the total embodied carbon, but the higher this contribution will be within the foundations.

Pie charts in Figure 3.6 show the contribution of the concrete and steel to the total embodied carbon within each structural system. Again, this representation is given for each typology and corroborates the previous observation on higher live load and the relatively lower contribution of the concrete within the slabs than within the foundations.

Figure 3.7 shows a parallel coordinate plot highlighting the following relationships between the model inputs and the total normalized embodied carbon of each design:

- For best performing designs: only the column concrete strength, floor-to-floor height, and soil-bearing capacity do not seem to have much impact. All the other features have specific ranges impacting the best-performing designs. In particular, the primary span, slab concrete strength, and live load are the top three most important features influencing these best-performing designs (the lower, the better). Moreover, designs including two-way slabs are more efficient than one-way systems, as demonstrated by the lower primary and secondary span ratio.
- Surprisingly, a higher number of floors leads to lower total embodied carbon in this dataset. This is because the roof in the parametric model is designed the same way as the floor slabs by assuming a two-way system which is seen in some types of incremental construction. However, since the roof is not considered to be occupied and is excluded from the total floor area, normalizing the embodied carbon of the structural system by the total floor area creates a penalty for smaller buildings (with two and three stories).

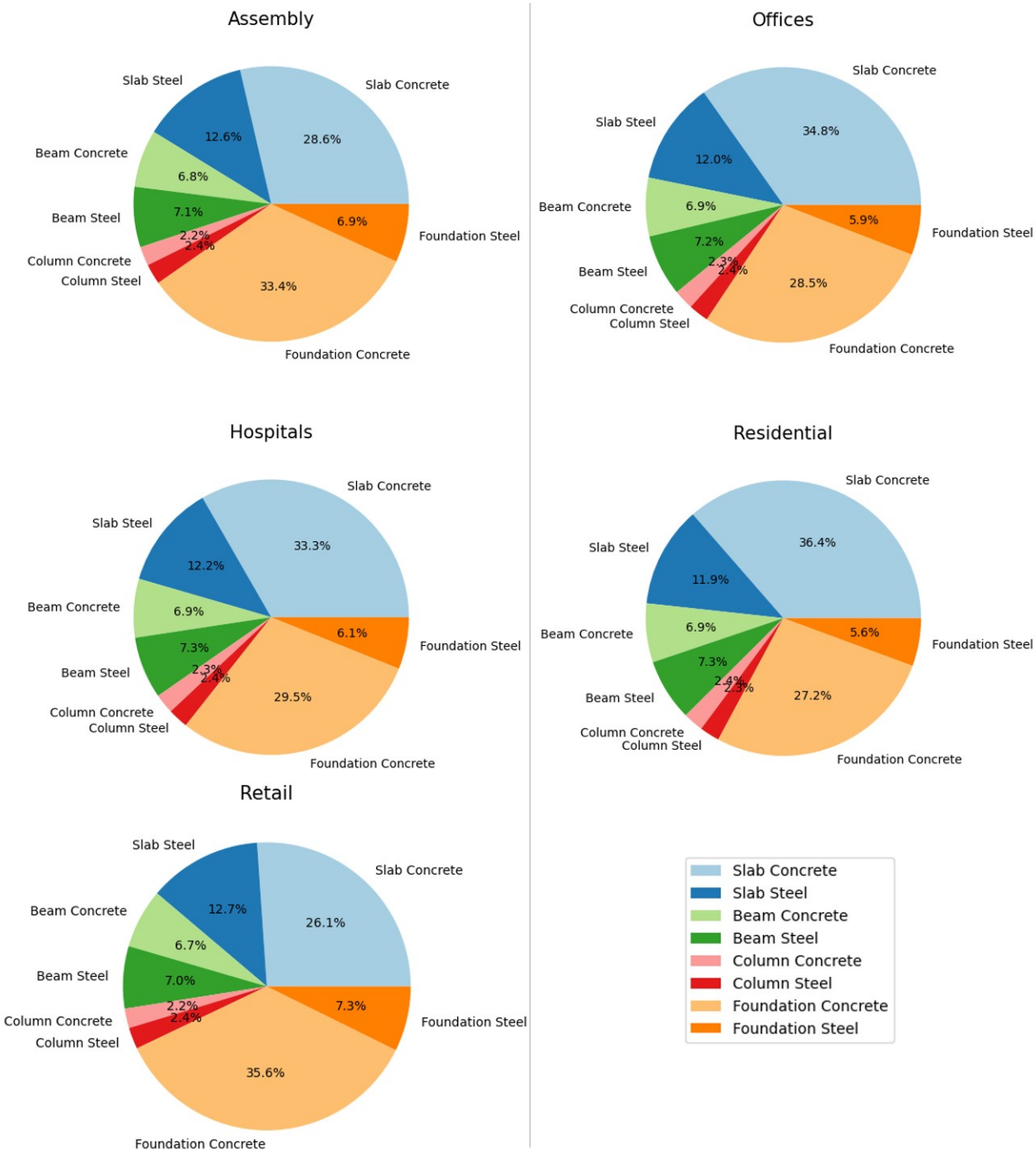

Figure 3.6: Contributions of Concrete and Reinforcing Steel in each Structural System.

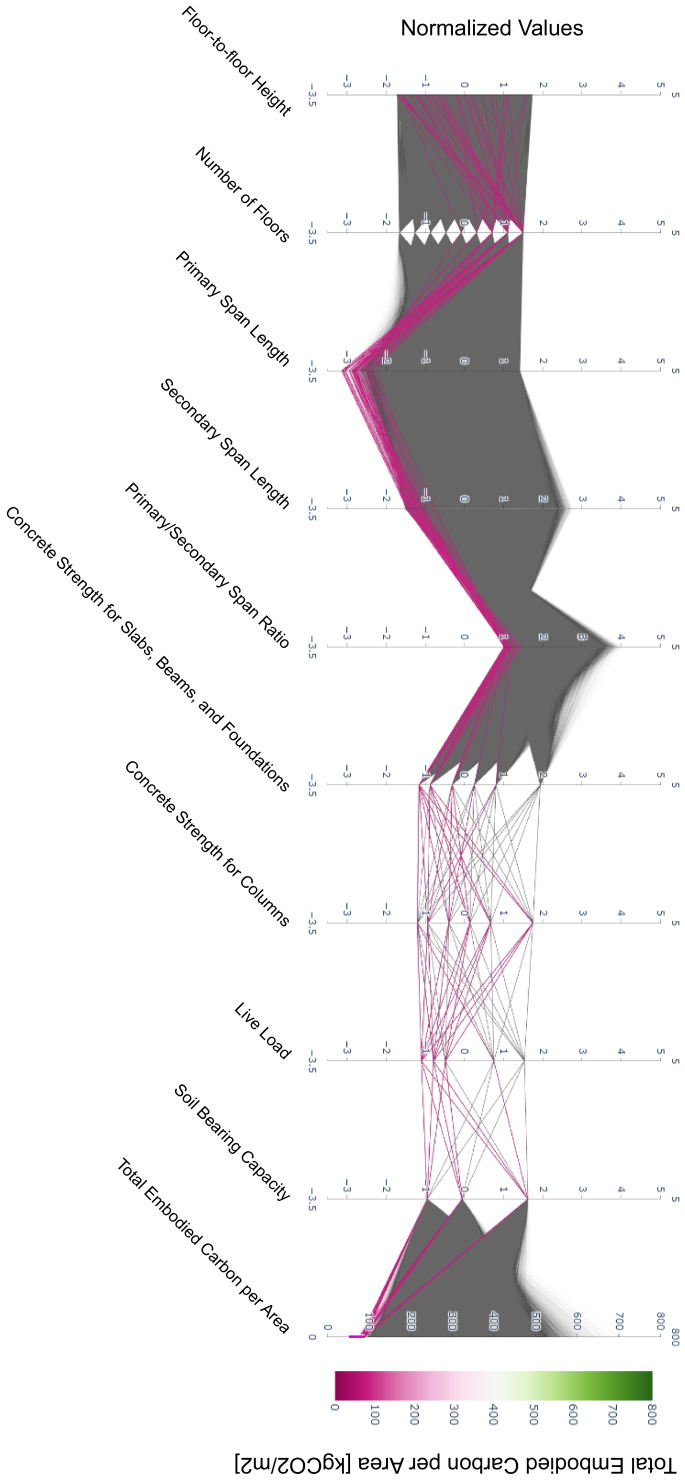

Figure 3.7: Parallel Coordinate Plot of the Model Normalized Inputs and Output.

3.3.2 Neural Network Validation

During validation, a total of nine neural network models were trained, and their performance was compared to select the best combinations of hyperparameters for the surrogate model. Table 3.3 summarizes the nine neural network models and their training and validation losses. The number of epochs was changed from a list of four values: 100, 200, 500, and 1000; the batch size was varied from values in the range: 500, 1000, and 2000; and the learning rate was tuned by comparing three values: 5e-5, 1e-4 and 1e-3. Overall, the best model calls for a batch size of 500, with a number of 1000 epochs and a learning rate of 1e-4. Amongst the other models, three were found to be overfitting.

Subsequently, Figure 3.8 presents the evolution of the training and validation losses of the best model, while Figure 3.9 displays the same graphs for two overfitting models.

Table 3.3: Training and Validation Losses Results.

Models	**Batch size**	**No. of epochs**	**Learning rate**	**MSE Training loss**	**MSE Validation loss**
1	1000	100	1e-4	0.033795	0.034463
2	1000	200	1e-4	0.022631	0.023259
3 (best)	**1000**	**500**	**1e-4**	**0.012886**	**0.015613**
4 (overfitting)	1000	1000	1e-4	0.010330	0.015643
5	500	500	1e-4	0.012460	0.017061
6	2000	500	1e-4	0.018528	0.022278
7 (overfitting)	2000	1000	1e-4	0.012217	0.015913
8 (overfitting)	1000	500	1e-3	0.004612	0.020922
9	1000	500	5e-5	0.011649	0.016086

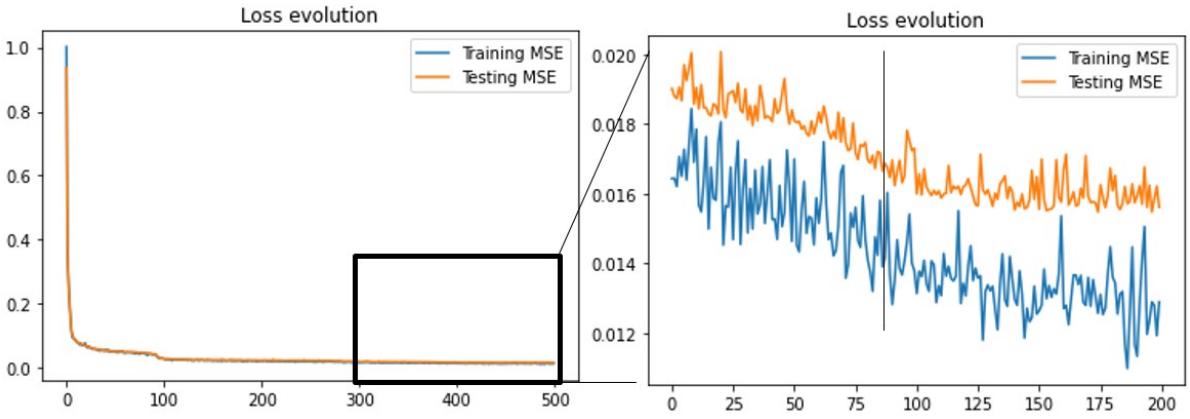

Figure 3.8: Loss Evolution Plot of the Best Neural Network Model.

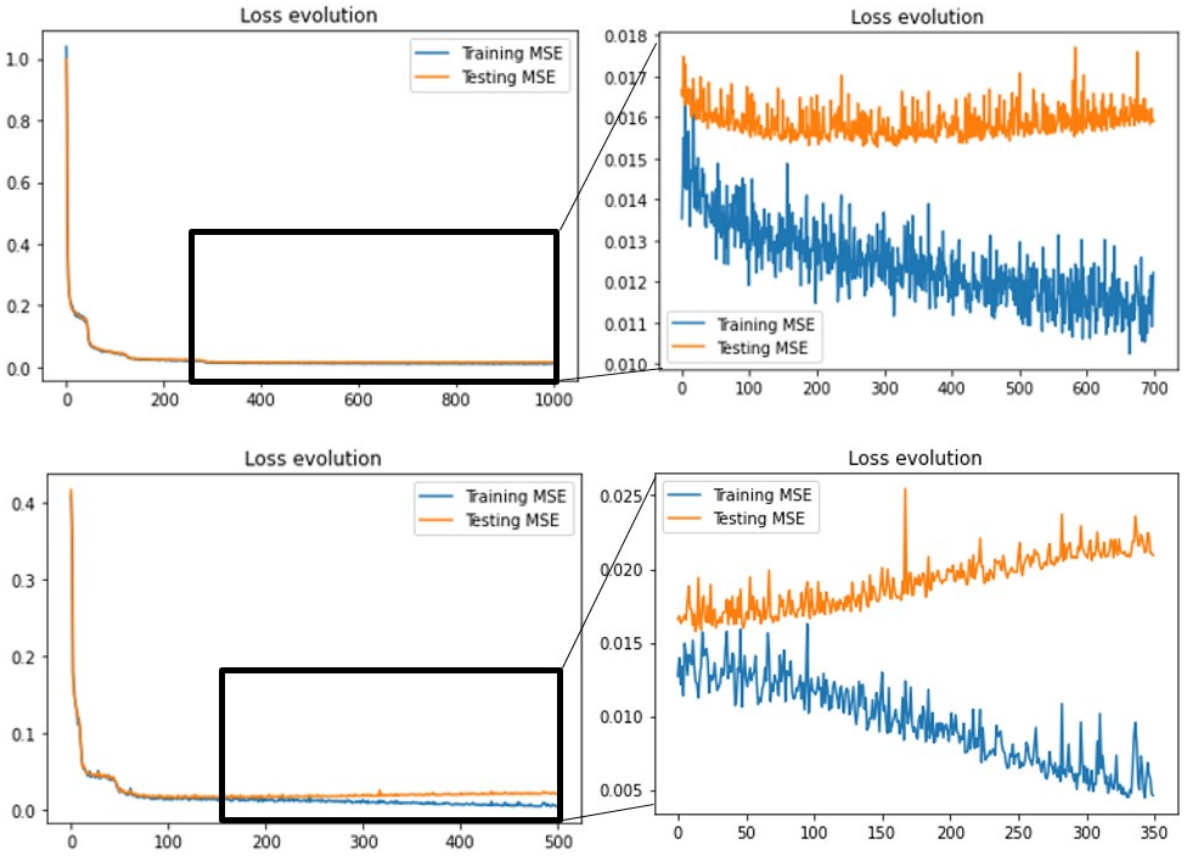

Figure 3.9: Loss Evolution Plot of two Overfitting Neural Network Models.

3.3.3 Neural Network Model Performance

Figure 3.10 shows the results of a feature importance study performed on the selected Neural Network model. To perform this analysis, the resulting changes in the output were calculated with respect to pertubations of each input feature. Then, the magnitude of these output changes served as the measure of feature importance for the corresponding input. This approach is referred to as a pertubation-based method. As anticipated from the parallel coordinate plot of the training data in Figure 3.7, the primary span, slab concrete strength, and live load remain, indeed, the most important features influencing the model.

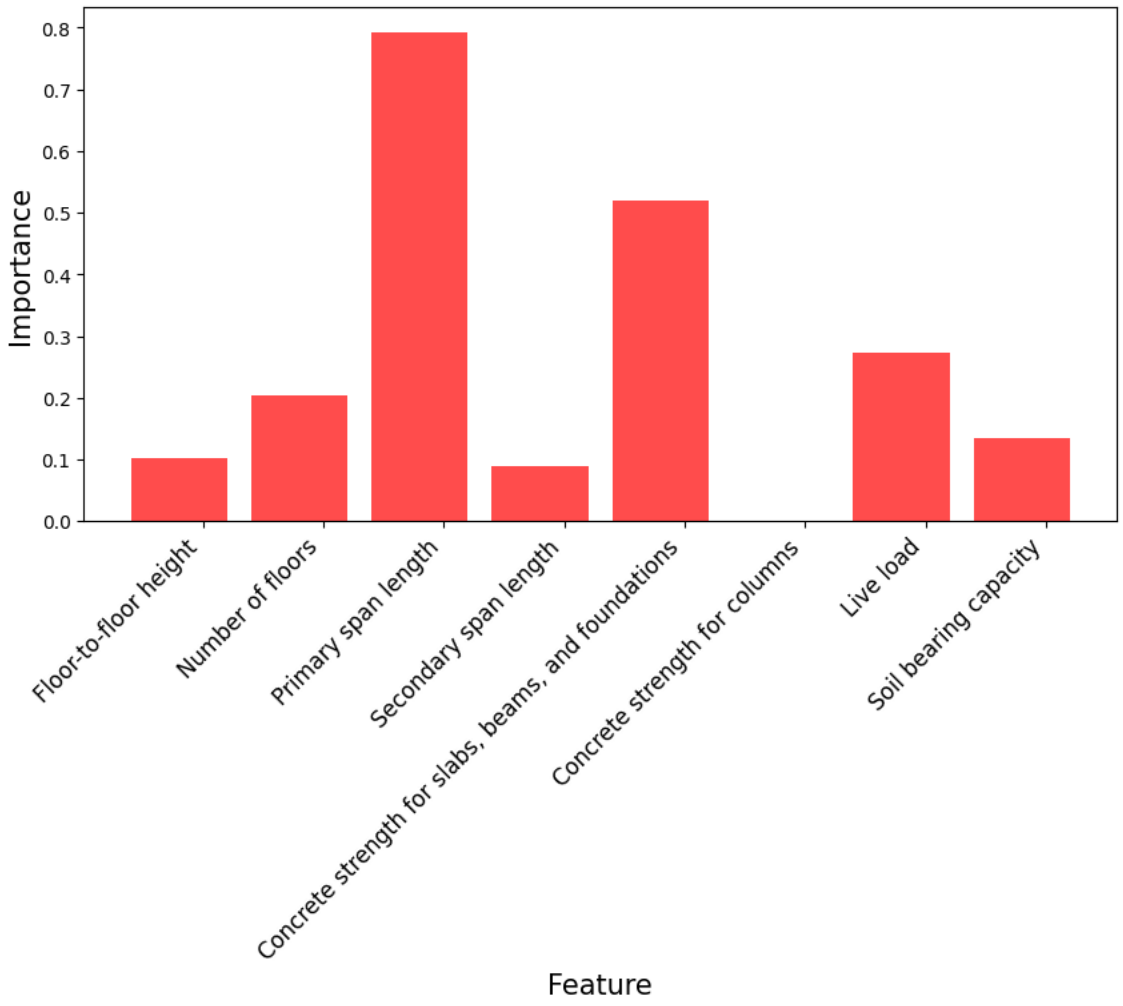

Figure 3.10: Neural Network Feature Importance.

Finally, Figure 3.11 presents prediction accuracy plots comparing the actual results from the parametric model with the predicted results obtained from the Neural Network model. Each data point represents the output of a specific design in each structural system and for both concrete (orange points) and steel reinforcement (green points). Overall, the data points align well with the central 1-to-1 line and remain within the 10 and 20% error bounds, which provides some confidence in the model performance. The next chapter discusses how to apply this model to urban modeling.

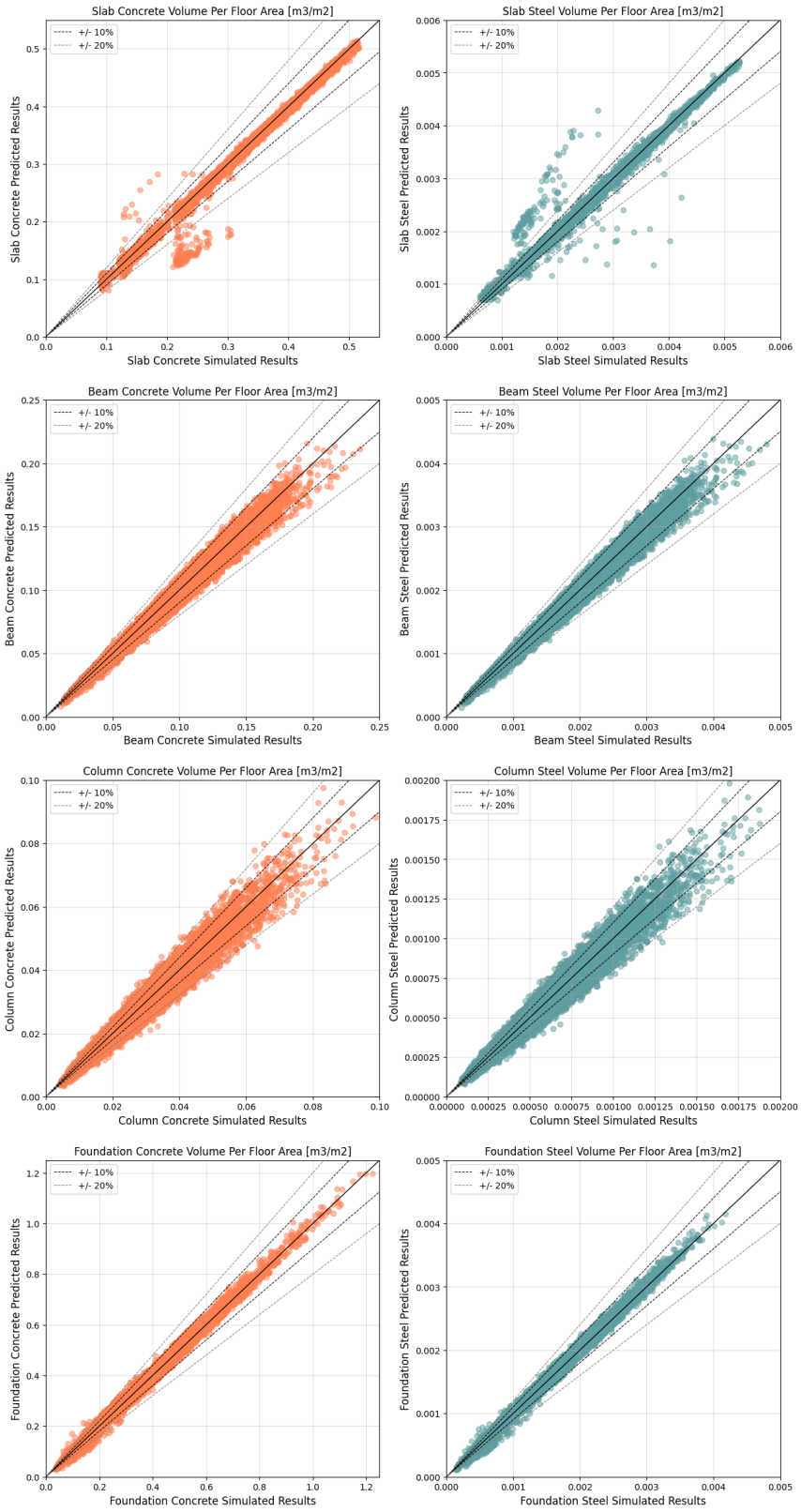

Figure 3.11: Neural Network Prediction Accuracy Plots.

Chapter 4

Applications into Urban Modeling of Embodied and Operational Carbon

This chapter describes the last part of the research methodology showing how to deploy the surrogate model and create building archetypes with structural parameters for urban-scale applications. As mentioned in the previous chapters, existing building archetypes only consist of a massing and an operational model. Adding structural parameters by creating an embodied model through this study allows the simulation of both embodied and operational carbon within the Urban Modeling Interface, as shown in Figure 4.1.

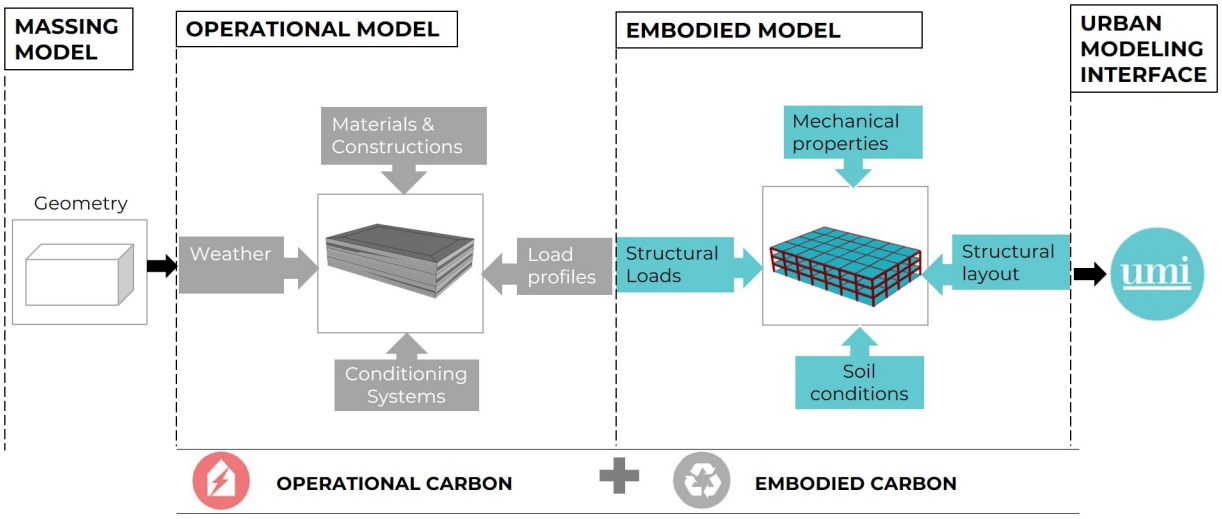

Figure 4.1: Structural Parameters Included to Define an Embodied Model within Building Archetypes.

Finally, the validity and feasibility of the methodology are assessed on two scales:

1. A whole-building scale using the Department of Energy (DOE) reference building templates through a sensitivity study on the impact of the column grid and concrete strength on embodied carbon intensity across archetypes.
2. A neighborhood scale through a case study based on real-world data from an existing building stock in Lisbon, Portugal, to assess the scenario of replacing the building stock with new construction and make recommendations on stock-level carbon reduction strategies.

4.1 Methodology for Integrating Structural Quantities Estimates into Urban Modeling

4.1.1 Framework for Deploying the Surrogate Model into UMI

One of the main advantages of using a surrogate model in early-stage design and/or urban modeling is its portability across frameworks, as demonstrated in Figure 4.2. After training, the Neural Network model can be exported with the obtained set of weights, model parameters, and hyperparameters and deployed into a different software tool to perform inferences. In this study, the surrogate model was trained in Python and deployed within a C-sharp application to allow its integration into UMI. To do so, the model was converted to an open standard format called ONNX (Open Neural Network Exchange) to ensure its interoperability (ONNX, 2023).

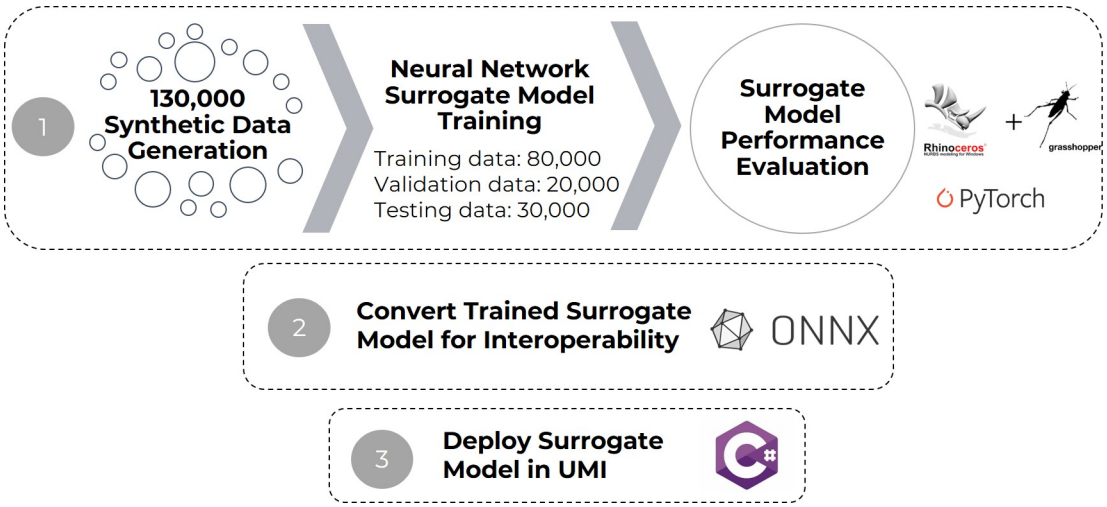

Figure 4.2: Three Steps for Deploying Surrogate Model into Urban Modeling Tool.

ONNX is a common file format used to represent machine learning and deep learning models so they can be deployed in a different inference environment than the training framework where they were originally developed. After the ONNX model is exported, its predictions are compared with the original Neural Network model to ensure both models yield the same results. Finally, ONNX Runtime is a tool used to load and run the ONNX model within the new environment. Moreover, ONNX Runtime provides improvement benefits to the model performance, such as a faster prediction speed.

4.1.2 Assumptions for Populating Embodied Model Structural Parameters

Integrating the trained surrogate model in the UMI Lifecycle module makes it possible to quickly estimate the embodied carbon in buildings' structural systems more accurately. Therefore, structural parameters specifying the live loading, materials from different construction systems, column grid layout, and soil conditions are added to the building archetypes and serve as inputs to the surrogate model integrated within UMI, as shown in Figure 4.3. This required significant updates to the UMI Lifecycle module C-Sharp code. Please refer to the UMI GitHub repository for more details related to these programming updates [1] (UMI, 2023).

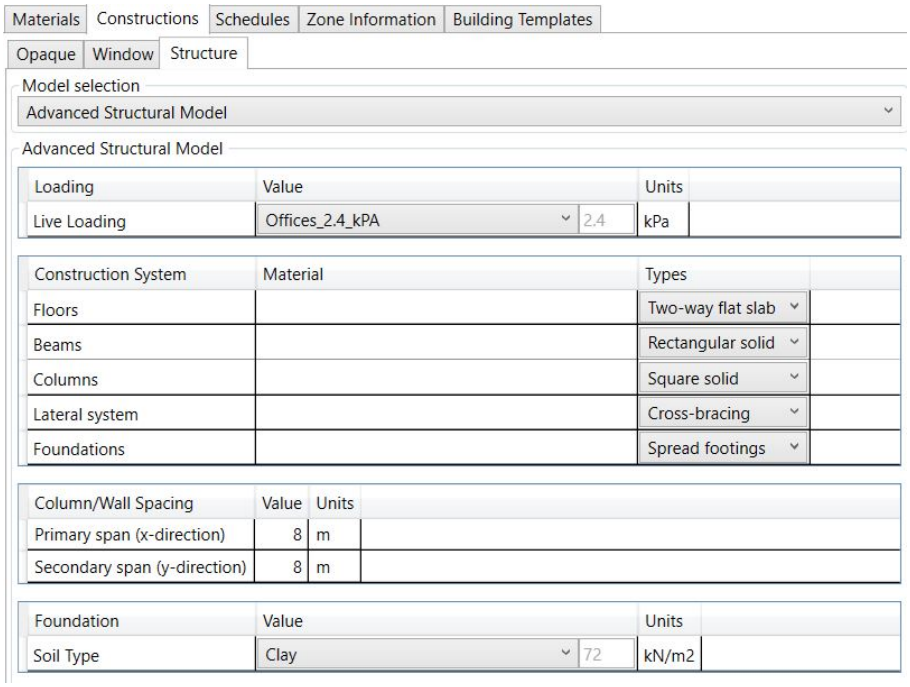

Figure 4.3: UMI User Interface Improvements to Include Structural Parameters for the Embodied Model.

[1] These changes were implemented with the help of Cody Rose (Research collaborator at the MIT Sustainable Design Lab).

Materials | Constructions | Schedules | Zone Information | Building Templates

Opaque | Glazing | Gas

Setting	Value	Units	Description	
Conductivity	1.75	W/mK		
Cost	0			
Density	2400	kg/m3		
Embodied Carbon	0	kgCO2/kg		
Embodied Energy	0	MJ/kg		
Substitution Rate Pattern	1			
Substitution Timestep	100			
Transportation Carbon	0.067	kgCO2/kg/km		
Transportation Distance	500	km		
Transportation Energy	0.94	MJ/kg/km		
Moisture Diffusion Resistance	50			
Roughness	Rough			
Solar Absorptance	0.7			
Specific Heat	840	J/kgK		
Thermal Emittance	0.9			
Visible Absorptance	0.7			
Design Strength	0	MPa		
Modulus of Elasticity	0	MPa		

Figure 4.4: Definition of the Synthetic Material Properties for Use in the Structural Model.

However, the module also maintains the existing workflow for the bottom-up estimation of all non-structural construction assemblies that comprise the building envelope (“Facade” and “Windows”) and interior elements such as “Partitions.” Therefore, all contributions of the structural materials within the “Ground,” “Roof,” and “Slab” construction assemblies are removed, as the surrogate model already accounts for them.To do so, a synthetic concrete material with zero embodied carbon coefficient and zero mechanical properties (design strength and modulus of elasticity) is defined in each archetype and used to avoid double counting the contribution of structural elements in the “Ground,” “Roof,” and “Slab,” as seen in Figure 4.4.

Another critical assumption when developing archetypes for embodied carbon estimation is to determine specific carbon intensity factors for electricity, oil, and gas in units of $kgCO_2e/kWh$. This is because the carbon intensity of electricity varies depending on the electricity mix of different regions. Therefore, specific factors for the selected region of our case study were calculated as follows.
First, carbon intensity factors of different energy sources for electricity generation were obtained in a recent LCA report published by the National Renewable Energy Laboratory (NREL) (Nicholson & Heath, 2021). Since region-specific data on the electricity mix was not found for the city of Lisbon, the electricity mix at the national level was obtained from an open-source database instead (OurWorldinData, 2023).

Then, the carbon intensity of electricity in Portugal was calculated to be 0.234 $kgCO_2e/kWh$ using a weighted average of the collected information. For oil and gas, intensity factors of 0.253 and 0.181 $kgCO_2e/kWh$ were directly taken from the US Environmental Protection Agency (EPA) data on carbon emissions coefficients per fuel (EPA, 2022).

After successfully setting up the structure necessary to deploy the surrogate model and include an embodied model in building archetypes for urban modeling, two case studies are analyzed in the remainder of this chapter.

4.2 Case Studies Description

4.2.1 Sample Models Definition and Sensitivity Analysis

The US DOE and NREL have established building templates for energy simulations of typical residential and commercial buildings (Reyna et al., 2022). Six reference building archetypes were considered to evaluate the performance of the surrogate model at the individual building level: a Single-family detached house, a Multi-family apartment building, a Medium office, a Primary school, a Stand-alone retail, and a (non-refrigerated) Warehouse. The characteristics of these sample models are presented in Table 4.1.

Table 4.1: Sample Models from DOE Residential and Commercial Prototype Buildings.

Archetypes	**Single-Family**	**Multi-Family**	**Medium Office**	**Primary School**	**Stand-alone Retail**	**Warehouse**
Live Load [kPa]	1.92	1.92	2.4	1.92	6	6
Total Floor Area [m^2]	442	3131	4985	7183	2299	4599
Length [m]	17.16	46.31	49.93	103.63	54.25	100.58
Width [m]	12.87	16.90	33.28	82.30	42.37	45.72
Number of Stories	2	4	3	1	1	1
Floor-to-floor Height [m]	3	3	4	4	6.1	8.5
Soil Type	Sand	Sand	Sand	Sand	Sand	Sand

Once defined within UMI, a sensitivity analysis was conducted on the chosen DOE reference building archetypes. Nine cases were obtained by simultaneously varying the column grid and concrete strength for each building typology, as shown in Table 4.2. Thus, yielding a total of 54 test cases. Selected results of the sensitivity study across four typologies (Multi-family, Single-family, Office, and Warehouse) and three cases (6x6 m grid & low concrete strength, 9x9 m grid & mid concrete strength, 12x12 m grid & high concrete strength) are presented in the following section. The complete results of this sensitivity analysis can be found in Appendix A.

Table 4.2: Sensitivity Study Cases Varying the Concrete Strength and Spacing Between Columns.

Case	**Concrete Strength [MPa]**			**Spans [m]**	
	Slabs, Beams & Foundations	Columns		Primary	Secondary
Case I	17.3	20.7	(Low)	6	6
Case II	17.3	20.7	(Low)	9	9
Case III	17.3	20.7	(Low)	12	12
Case IV	27.6	34.5	(Mid)	6	6
Case V	27.6	34.5	(Mid)	9	9
Case VI	27.6	34.5	(Mid)	12	12
Case VII	41.3	55.1	(High)	6	6
Case VIII	41.3	55.1	(High)	9	9
Case IX	41.3	55.1	(High)	12	12

4.2.2 Lisbon Case Study Definition

The methodology was finally applied to a large-scale case study in the city of Lisbon, Portugal[2]. It is important to note that the current goals set by the city of Lisbon are to reduce its carbon emissions by 60% by 2030 and reach carbon neutrality by 2050 (International Energy Agency, 2021). Therefore, this study aims to determine the spatial distribution of embodied and operational carbon in a neighborhood representative of the Lisbon building stock to inform policy and planning decisions on retrofitting strategies and new construction.

A seed model of a neighborhood referred to as the C-Tech area served as the focus area of the case study. The C-Tech area is located in the northeastern part of Lisbon along the Tagus River and spans three parishes or neighborhoods: Parque das Nacoes, Marvila, and Beato. This case study introduces seven building archetypes based on a specific construction period from 1961 to 1980. This specific construction period was marked by rapid and intense construction activities in Lisbon - specifically, a boom in reinforced concrete constructions. Most of these constructions are now approaching the end of their life. Figure 4.5 illustrate typical examples of these buildings.

The context of this case study is particularly appropriate since half of the buildings in Lisbon include a reinforced concrete structure. In addition, about 70% of these buildings were designed before 1980 to sustain gravity loading only, as the role of the lateral load system for seismic resistance was introduced in the building code in 1983 (Xavier et al., 2022). Therefore, the scope of this case study is limited to low- and mid-rise reinforced concrete buildings below ten stories. The surrogate model from this methodology is trained to perform accurate early-stage predictions of structural quantities provided similar constraints.

[2]This case study was made possible thanks to a collaboration between the MIT Sustainable Design Lab, the Instituto Superior Técnico (IST) in Lisbon, and local organizations through the MIT Portugal Program.

(a) (b)

Figure 4.5: Photos from 1961-1980 Typical Reinforced Concrete Buildings and Floor Plans in Lisbon (Xavier et al., 2022).

Thus, the research questions that emerge from this case study are two-fold:

1) How much embodied and operational carbon would this building stock generate if it were built again today?
2) Is it worth constructing new buildings to replace old carbon hotspots, or should these existing buildings be retrofitted?

First, reliable building archetypes were created to measure the embodied carbon and energy use intensities at the stock level within the C-tech area, assuming all buildings would be replaced today. Second, a comparison was made between the case study baseline results and existing benchmarking studies presented in Chapter 2 to quickly identify the buildings better suited for replacement or retrofitting. Retrofitting strategies per se are not evaluated in this study, but some recommendations on whether to conduct a deep or shallow retrofit are given.

The segmentation of the building stock into archetypes was based on GIS data available for this neighborhood. In addition, more data was collected to specify reasonable structural parameters for each archetype from existing studies characterizing the Lisbon building stock (Xavier et al., 2022) and rules of thumb from local construction practices adopted by architects and engineers. For example, different structural grids were considered based on the typical spans of reinforced concrete beams across different typologies. When defining the building archetypes, the soil was assumed to be mainly composed of sand, even though there is undoubtedly much more variability in reality. Table 4.3 summarizes the building archetypes' structural parameters defined for this case study.

Different urban energy modeling archetypes have been studied extensively in Lisbon for residential, office, and retail typologies (Monteiro et al., 2017). These existing archetypes served as a reference to define the parameters of the operational models used in this case study, shown in Table 4.4. It should be noted that the Parking archetype was considered an unconditioned space with no heating, cooling, mechanical ventilation, or domestic hot water loads.

Table 4.3: Definition of Archetypes Structural Parameters for Lisbon Case Study.

Archetypes	**Single Family**	**Multi Family**	**Office**	**School**	**Retail**	**Ware-house**	**Parking**
Count	619	621	128	78	29	14	157
Live load [kPa]	1.92	1.92	2.4	1.92	6	6	1.92
Floor-to-floor height [m]	3	3	4	4	6.1	8.5	3
Concrete strength [MPa] (slabs, beams, foundations)	17.3	17.3	20.7	17.3	20.7	27.6	27.6
Concrete strength [MPa] (columns)	20.7	20.7	27.6	20.7	27.6	34.5	34.5
Primary span [m]	4	5	8	9	10	12	12
Secondary span [m]	3	5	8	9	10	6	8
Soil type	Sand	Sand	Sand	Sand	Sand	Sand	Sand

Table 4.4: Definition of Archetypes Operational Model Parameters for Lisbon case study.

Archetypes	**Single Family**	**Multi Family**	**Office**	**School**	**Retail**	**Ware-house**	**Parking**
Occupancy density [p/m^2]	0.025	0.025	0.055	0.2	0.1	0.001	0.001
Equipment power density [W/m^2]	4	4	8	16	6	3	1
Lighting power density [W/m^2]	7	7	12	12	12	5	5
Heating COP	1	1	1	1	1	1	-
Cooling COP	3	3	3	3	3	3	-
Infiltration rate [ACH]	0.35	0.35	0.35	0.35	0.35	0.35	0.35
Ventilation	Natural	Natural	Mech.	Mech.	Mech.	Mech.	-

The embodied carbon emissions from the replacement of the Lisbon building stock today were compared to data from the Embodied Carbon Benchmarking (ECB) database by Simonen, Rodriguez, and De Wolf (2017) and the EU-Embodied Carbon Benchmarking (EU-ECB) study by Röck and Sørensen (2022). It was essential to ensure a fair comparison with the chosen benchmarking studies. Since the ECB database covers embodied carbon emissions from Life Cycle stage A across different buildings' heights, the benchmarks selected for the comparison were associated with buildings with less than 14 stories and thus were assumed only to include a gravity system. Similarly, as the harmonized data from the EU-ECB study cover whole-lifecycle embodied emissions, specific benchmarks for cradle-to-gate embodied carbon were derived using the mean contribution of the lifecycle product stage A1-A3 estimated at 56%.

4.3 Results and Discussion

4.3.1 Sensitivity Analysis Results

Selected results from the Multi-family, Single-family, Medium office, and Warehouse sample models are compared. Figures 4.6 to 4.9 show the embodied carbon intensity (ECI) breakdown from the concrete and steel in the Structure (including slabs, beams, columns, and foundations) and other non-structural materials in the Envelope and Interior. Since this sensitivity study is focused on varying the parameters of the structural systems, no variations appear in the embodied carbon intensities of the Envelope and Interior within each typology. However, as the column grid takes on larger spans, the proportion of the total embodied carbon intensity from the Envelope and Interior is reduced compared to that of the Structure. In addition, as the concrete strength increases, the embodied carbon increases due to the Structure. In particular, the changes in embodied carbon intensities within the foundations are greater than within the slabs, beams, and columns.

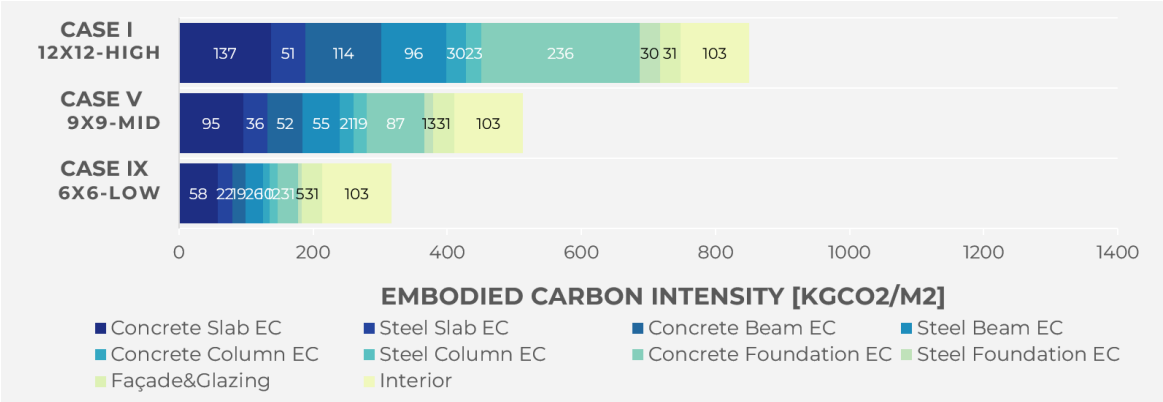

Figure 4.6: Multi-Family Sensitivity Study Results for Selected Cases I, V, and IX.

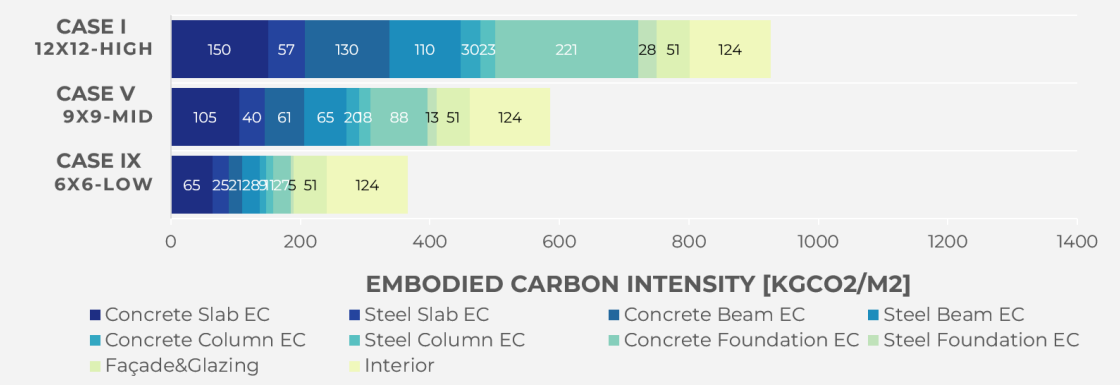

Figure 4.7: Single-Family Sensitivity Study Results for Selected Cases I, V, and IX.

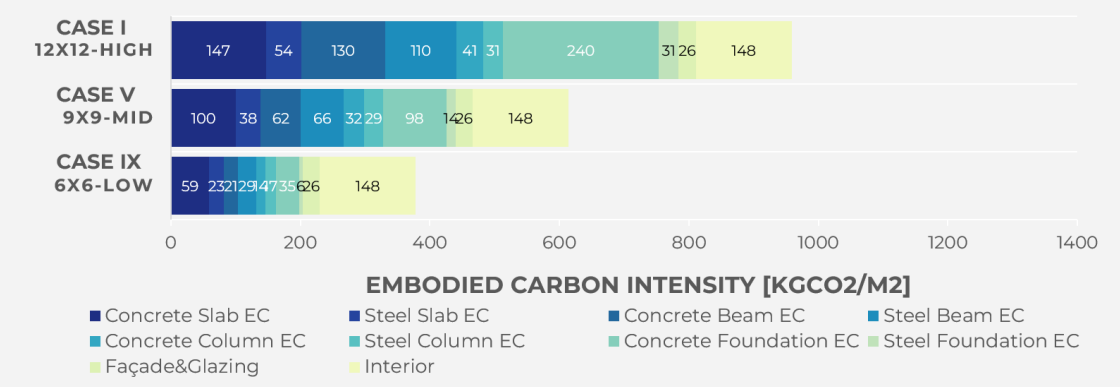

Figure 4.8: Office Sensitivity Study Results for Selected Cases I, V, and IX.

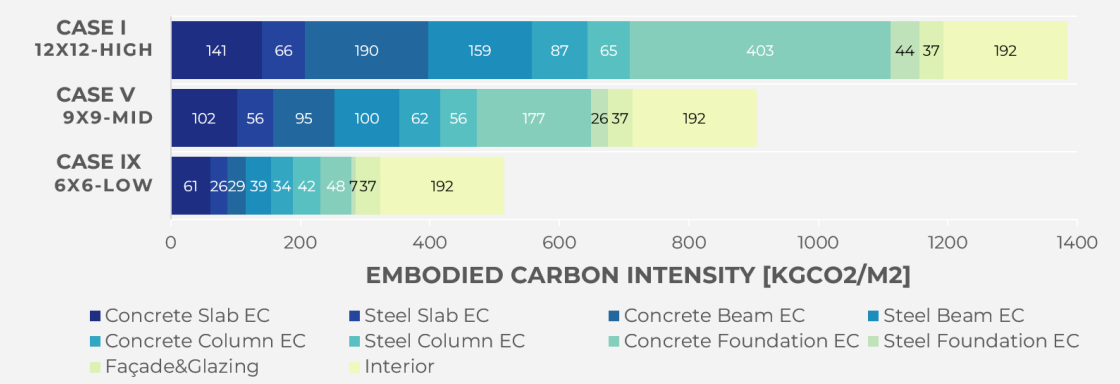

Figure 4.9: Warehouse Sensitivity Study Results for Selected cases I, V, and IX.

4.3.2 Case Study Results

Figures 4.10 and 4.11 present the spatial distribution of the upfront embodied carbon and annual operational energy use intensities obtained through UMI.

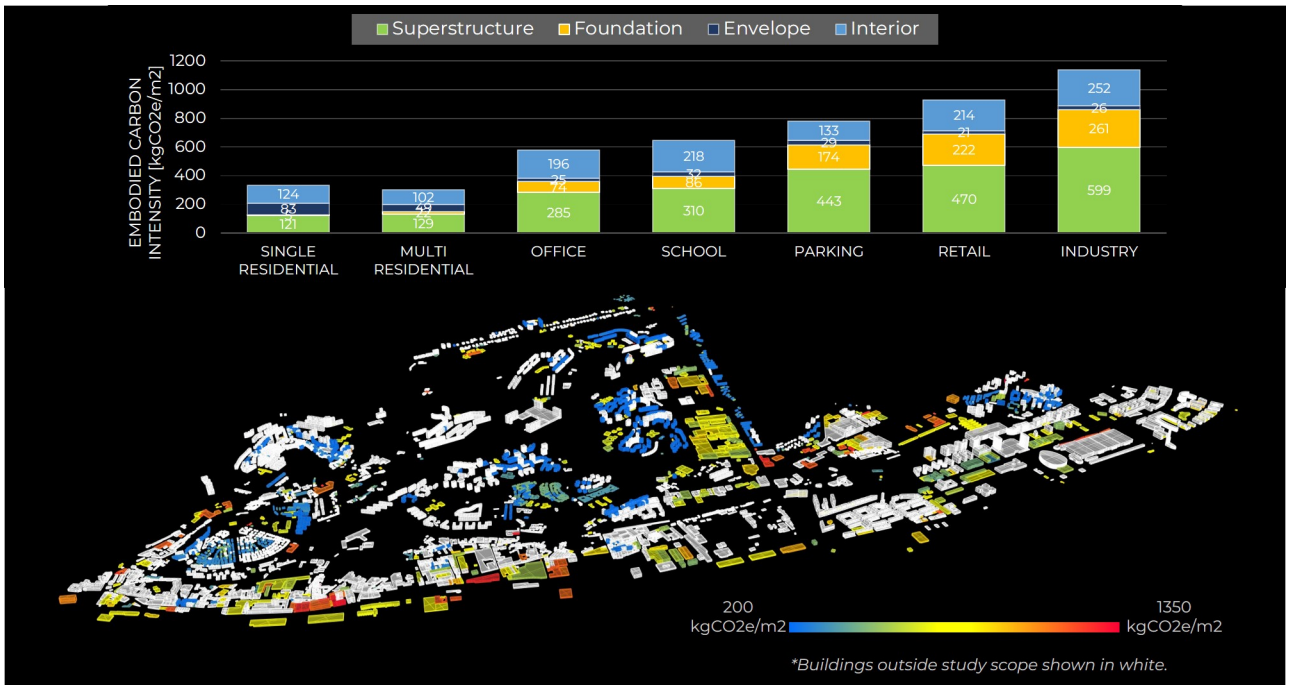

Figure 4.10: Spatial Distribution of Embodied Carbon Intensity.

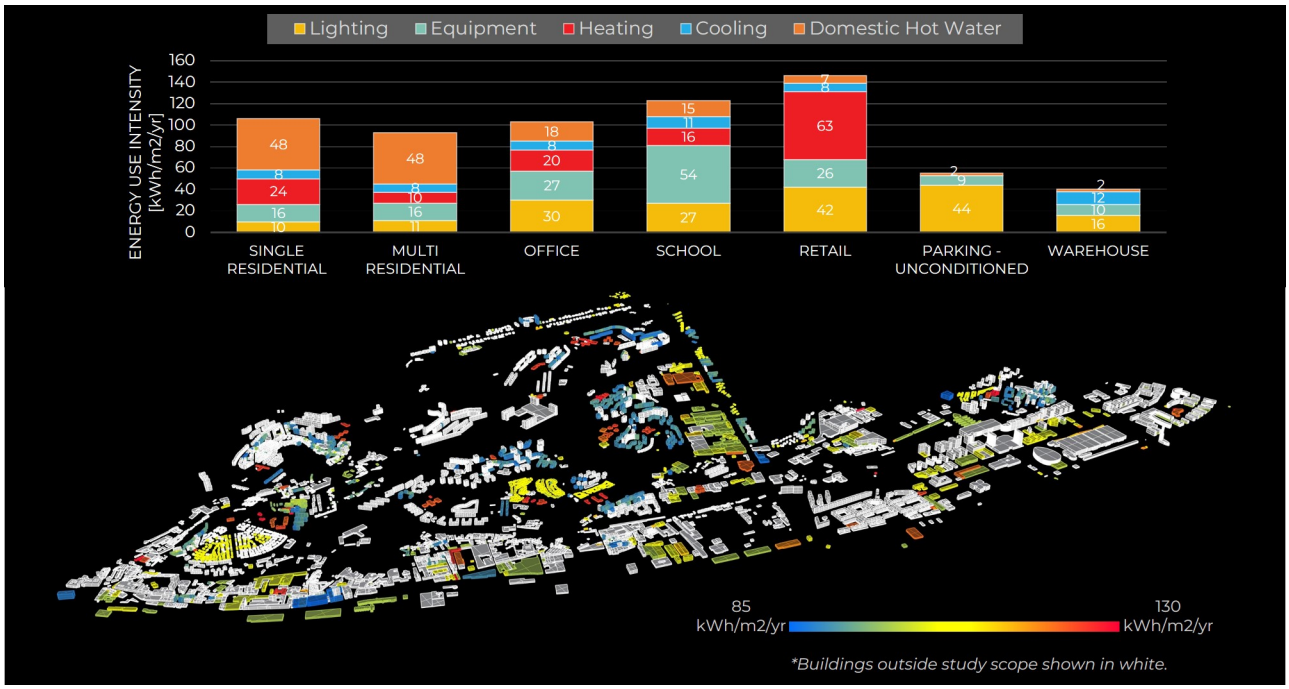

Figure 4.11: Spatial Distribution of Energy Use Intensity.

The urban-level simulation for the Lisbon case study included 1646 buildings and only took one minute to run in UMI. The rest of the building massings outside the scope of the case study were treated as shading objects in the operational energy analysis. If built again today, the average embodied carbon intensity of the entire site is estimated at 416 $kgCO_2e/m^2$ while the annual operational energy intensity is 98 $kWh/m^2/yr$, which translates to an annual operational carbon intensity of 21 $kgCO_2e/m^2/yr$.

4.3.3 Comparison with Embodied Carbon Benchmarking Studies

In their benchmarking study, Simonen et al. concluded that over 95% of buildings reported upfront embodied carbon values lower than 1000 $kgCO_2/m^2$ for the building structure, foundation, and enclosure (Simonen et al., 2017). As shown in Table 4.5, most of the archetypes of the Lisbon case study agree with this finding, except for the Retail and Warehouse. For Retail, a little less than 75 % of buildings were found to have an embodied carbon intensity below 1000 $kgCO_2/m^2$. And for the Warehouse, only 10% of buildings ECI were below 1000 $kgCO_2/m^2$, as most of them had upfront embodied carbon intensities above this threshold.

Moreover, different benchmarks for commercial and residential buildings are highlighted within the ECB study. 50% of commercial office buildings in the database have an embodied carbon ranging from 200 and 500 $kgCO_2/m^2$. Low-rise residential buildings have an upfront embodied carbon typically lower than 500 $kgCO_2/m^2$. In the Lisbon case study, all residential archetypes meet this limit. However, in the results obtained from Lisbon, 50% of office buildings have an upfront embodied carbon intensity between 459 and 568 $kgCO_2/m^2$, which is a tighter range than that of the ECB findings.

Table 4.5: Embodied carbon intensity (ECI) extremes and percentiles per archetype in the Lisbon case study.

Archetype	**Extremes and percentiles of embodied carbon intensity**				
	Min	25^{th}	50^{th}	75^{th}	Max
Single Family	250	298	327	358	500
Multi Family	253	275	287	314	515
Office	459	518	568	630	877
School	505	593	643	676	945
Retail	793	854	904	1016	1109
Warehouse	982	1051	1101	1183	1518
Parking	632	715	763	818	1094

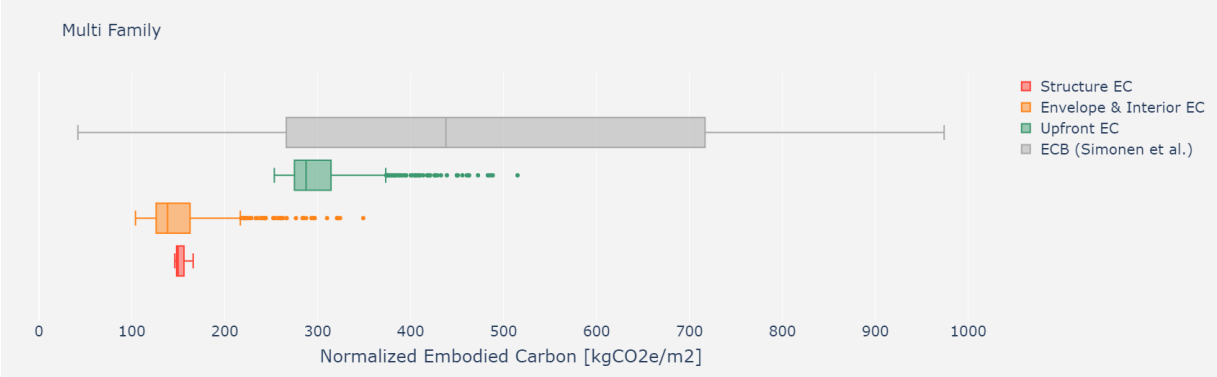

Figure 4.12: Comparison of Multi-Family Benchmark Between Lisbon Case Study and ECB Database.

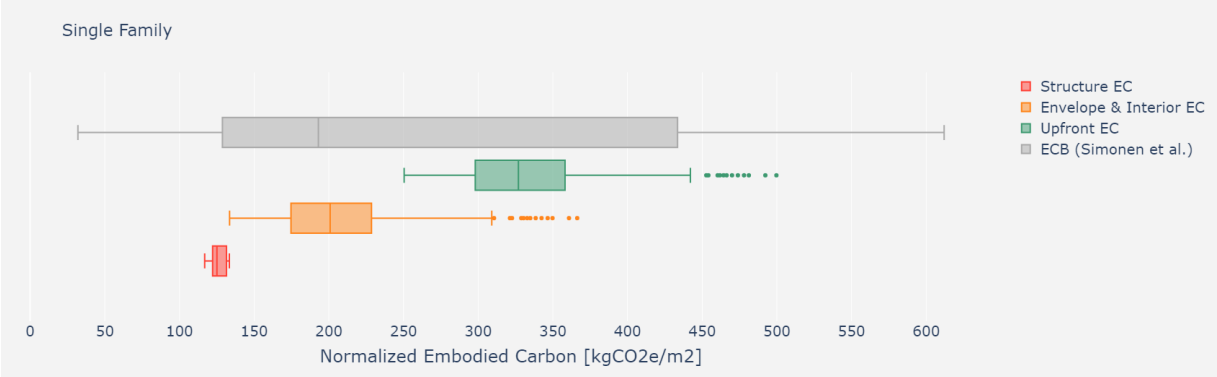

Figure 4.13: Comparison of Single-Family Benchmark Between Lisbon Case Study and ECB Database.

Figures 4.12 to 4.18 compare the Lisbon case study results with the ECB study using box-and-whisker plots to display the distribution of embodied carbon intensity values. Grey boxplots refer to the ECB study. Results from the Lisbon case study are broken down into three boxplots. The embodied carbon intensities of the Structure, and Envelope, and Interior are separated as red and orange boxplots, respectively. Finally, the total upfront ECI from the case study is shown as a green boxplot.

For most archetypes, the upfront embodied carbon intensity range in this case study is much smaller than the range taken from the ECB database. Moreover, due to the definition of specific structural parameters in building archetypes, the Structure ECI shows smaller variations than the Envelope and Interior for all archetypes, as red boxplots are shorter than the orange ones. The Structure ECI results have little to no outliers across all typologies, whereas the Envelope and Interior ECI have noticeable outliers for residential archetypes. For the Multi-family and Single-family archetypes, it can be noted that the median structure ECI is about the same or lower than the median ECI of the Envelope and Interior. Therefore, the Envelope and Interior contribution to the upfront ECI is about the same for Multi-family and higher for Single-family than the Structure.

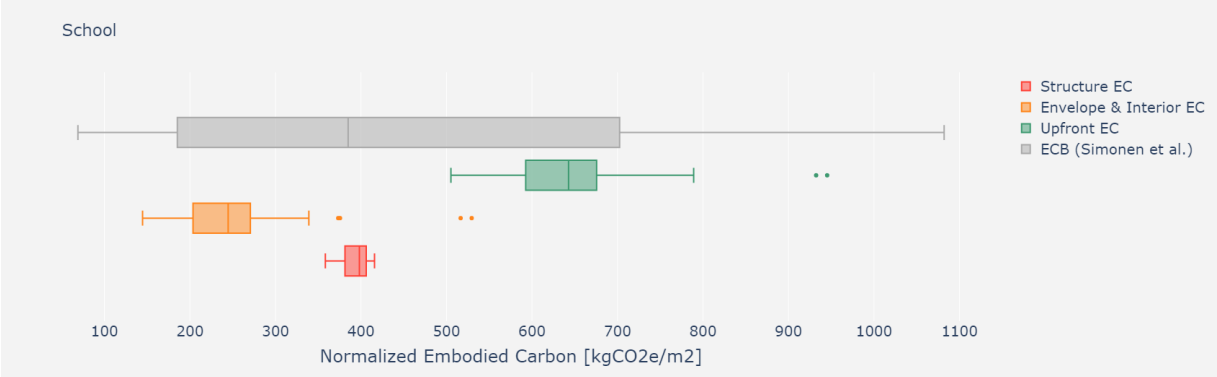

Figure 4.14: Comparison of School Benchmark Between Lisbon Case Study and ECB Database.

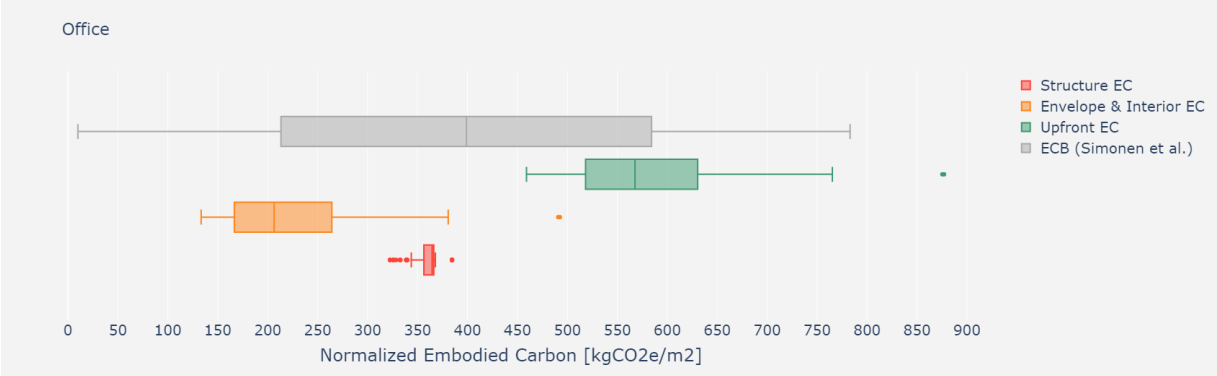

Figure 4.15: Comparison of Office Benchmark Between Lisbon Case Study and ECB Database.

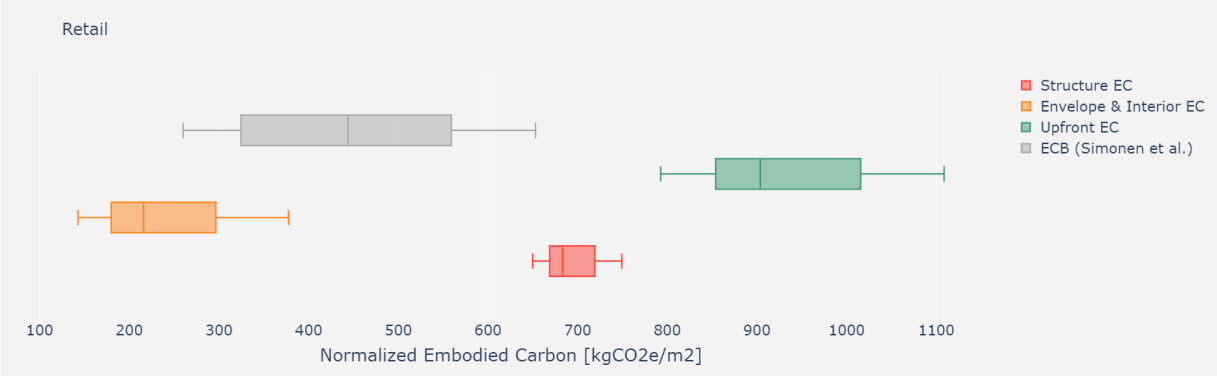

Figure 4.16: Comparison of Retail Benchmark Between Lisbon Case Study and ECB Database.

In the case of the School and Office archetypes, the range of ECI of the Structure is higher than for the Envelope & Interior. Thus, as the live load increases, the Structure has a

larger contribution to a building's upfront embodied carbon. When comparing the results of the two studies for the Retail archetypes, it appears that using benchmarks from the ECB survey underestimates the upfront ECI in Lisbon. The Warehouse and Parking archetypes were defined to have structural parameters with the highest concrete strength and primary span. Therefore, the Structure ECI is significantly greater than the Envelope & Interior.

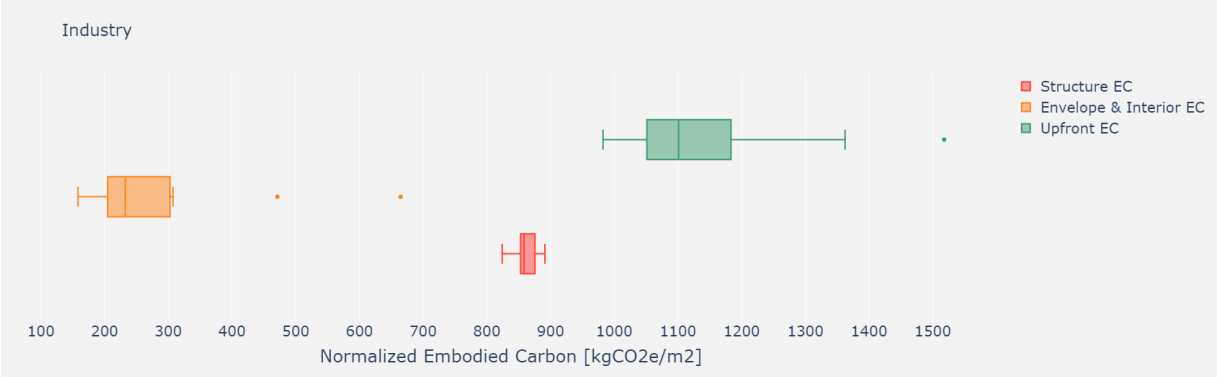

Figure 4.17: Warehouse Benchmark in Lisbon Case Study.

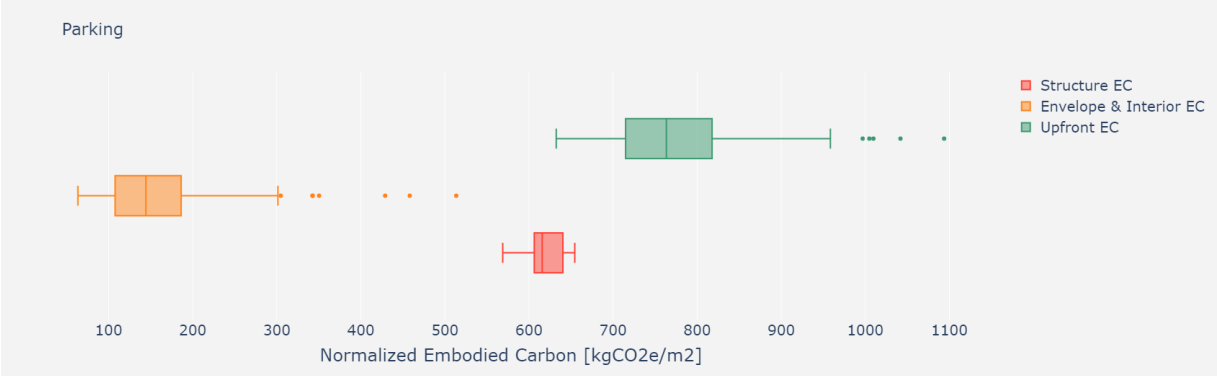

Figure 4.18: Parking Benchmark in Lisbon Case Study.

Table 4.6 and 4.7 show the results of the Lisbon case study and how it compares with the harmonized data from the EU-ECB database. It can be noted that the mean contribution of the Superstructure to the upfront embodied carbon increases with the live loading, concrete strength and column grid. Indeed, in Table 4.6, the Warehouse has the highest live loading and its Superstructure is shown to account for 53% of the upfront embodied carbon while the reverse is true for the Single-family archetype. Besides, Parking has the highest contribution from the Structure at 57% since it has the largest column grid spacing and uses the highest concrete strength. The contribution of the Foundation increases more rapidly than the Superstructure as it jumps from only 2% of the embodied carbon intensity of the Single-family to 24% for the Retail archetype. In contrast, the contribution of the Envelope and Interior varies from 62 % in Single-family to 21% in Parking. The ef-

ficiency of the Multi-family Envelope against that of the Single-Family is also apparent in this analysis. All of these findings agree with the results from the sensitivity analysis at the individual building level.

Table 4.6: Table of Mean Embodied Carbon Intensity (ECI) Results from the Lisbon Case Study per Building System for each Typology.

Mean ECI	**Superstructure**		**Foundation**		**Envelope & Interior**		**Total**
Archetype	Absolute	Relative	Absolute	Relative	Absolute	Relative	Absolute
Single Family	121	36%	5	2%	207	62%	333
Multi Family	129	43%	22	7%	151	50%	302
Office	285	49%	74	13%	221	38%	580
School	310	48%	86	13%	250	39%	646
Parking	443	57%	174	22%	162	21%	779
Retail	470	51%	222	24%	235	25%	927
Warehouse	599	53%	261	23%	278	24%	1138

Table 4.7: Table of Mean Embodied Carbon Intensity (ECI) Results per Building System from the Lisbon Case Study and EU-ECB Study.

Mean ECI	**Superstructure**		**Foundation**		**Envelope & Interior**		**Mechanical**	
Archetype	Mean	% Diff	Mean	% Diff	Mean	% Diff	Mean	% Diff
EU-ECB	170		50		260		230	
Lisbon	187	5%	43	8%	186	17%	-	-

Table 4.7 reveals that the ECI results for the Superstructure and Foundation in the Lisbon case study are comparable to the benchmarks form the EU-ECB database, as demonstrated by relative differences of 5% and 8% between both studies. However, there are larger differences with the Envelope and Interior, which result in a relative difference of 17 %. The EU-ECB database also includes the embodied carbon emitted by the mechanical systems which is outside of the scope of the Lisbon case study.

Figure 4.19 shows the comparison of ECI between EU-ECB and all the buildings in the case study broken down in three categories (Superstructure, Foundation, and Envelope and Interior) in the form of whisker and boxplots. Please note that outliers from the EU-ECB report are not shown in this graph. The results of the Lisbon benchmarks fall within the range of data of the EU-ECB study (excluding outliers) for the Foundation and Superstructure. Whereas, the distribution of data for the Envelope and Interior in the Lisbon case study does not match with that of the EU-ECB database.

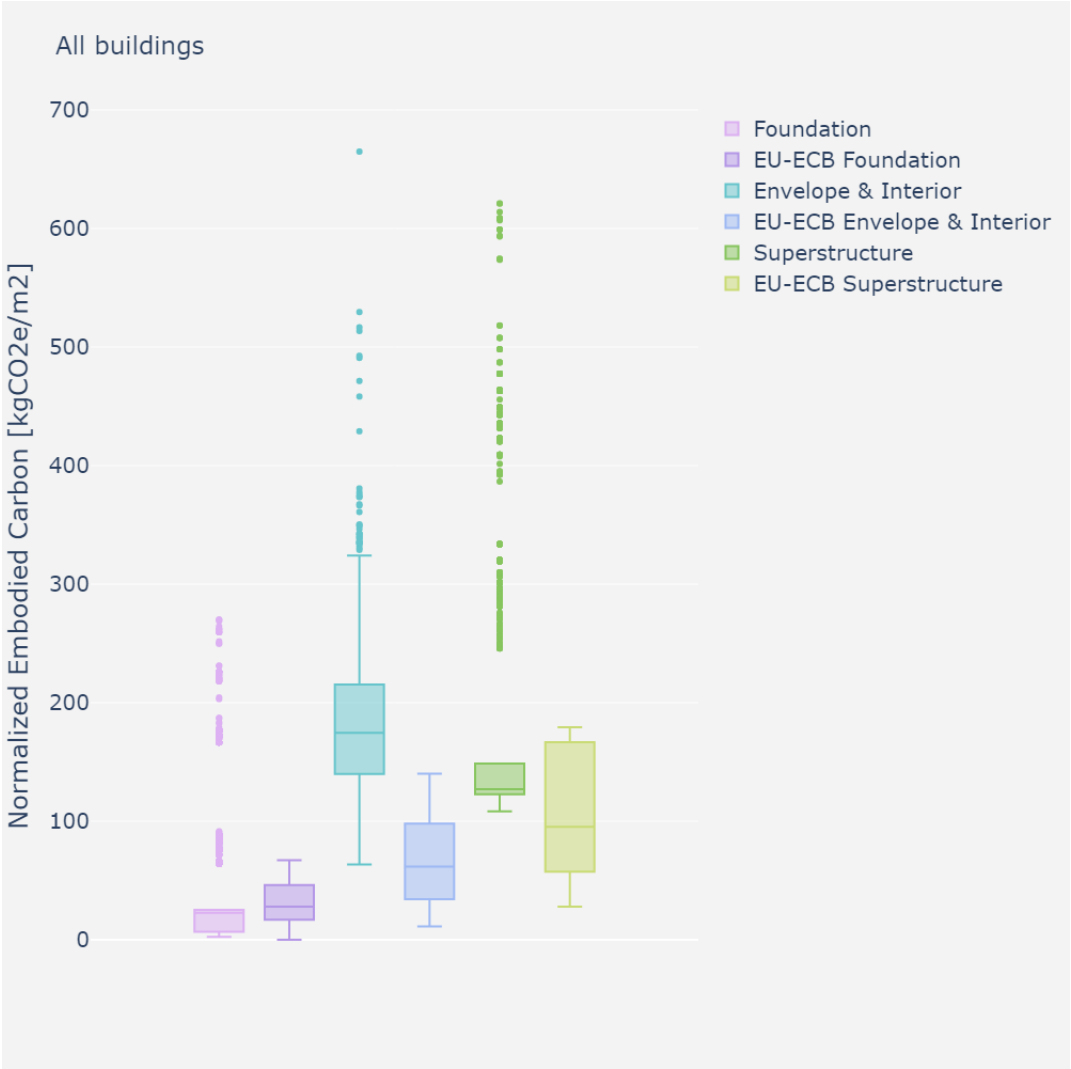

Figure 4.19: Comparison of Structure Benchmark Between Lisbon Case Study and EU-ECB Database.

4.3.4 Recommendations for Decision-making in Case Study

To conclude the case study, a framework of stock-level recommendations is developed to inform decision-making while considering the tradeoffs between operational energy and embodied carbon intensities from the baseline results. As shown in Figure 4.20, this framework allows to classify buildings within four distinct categories.
First, based on whether their energy use intensity exceeds the mean of the entire building stock, they are divided into two categories of buildings: “High Operational Energy” and “Low Operational Energy.” Each category is then subdivided based on the buildings’ embodied carbon intensity to define two additional sub-categories: “High Embodied Carbon” and “Low Embodied Carbon.”

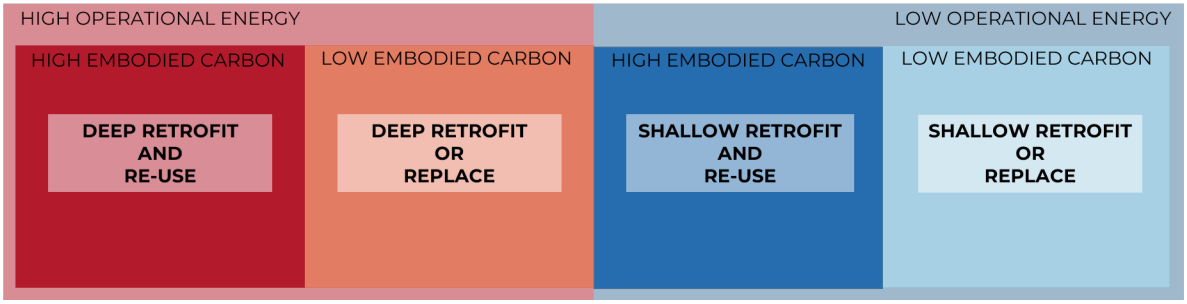

Figure 4.20: Framework for Decision-making Recommendations Based on Tradeoffs Between Operational Energy and Embodied Carbon.

Therefore, buildings belonging to Category I (High Operational Energy and High Embodied Carbon) are excellent candidates for a “Deep Retrofit and Reuse” strategy. Applying this strategy can prevent significant carbon emissions associated with new construction. Buildings in Category II (High Operational Energy and Low Embodied Carbon) can be considered either for a “Deep Retrofit” or a “Replacement” strategy. In both cases, the carbon footprint of these buildings can be lower than the current building stock average, with a deep energy retrofit or with a new low-carbon construction.

However, further analysis would be required in Category II to select the most appropriate and feasible strategy considering additional technological and socioeconomic factors. For example, a deep energy retrofit might be sufficient to reduce energy use in an existing building, yet too expensive or unfeasible given its context. Therefore, rebuilding a low-carbon and energy-efficient new design might be more beneficial. In contrast, a historical building might be more suited for a deep retrofit if it represents a symbol for the community, who might disapprove of its demolition.

Similarly, buildings in Category III (Low Operational Energy and High Embodied Carbon) would benefit from a “Shallow Retrofit and Reuse” strategy, while buildings in Category IV (High Operational Energy and High Embodied Carbon) could be subjected either to a “Shallow Retrofit” or a “Replacement” strategy. Since shallow retrofits are easier to implement than deep retrofits, recommendations in Categories III and IV can be faster to execute. At the same time, recommendations associated with buildings in categories I and II would have a greater impact on reducing annual operational carbon.

Based on this framework, the spatial distribution of the Lisbon case study building stock is shown in Figure 4.21. Moreover, the different proportions of buildings that fall within each category of recommendations are given. Office, School, and Retail archetypes were shown to require the “Deep Retrofit and Reuse” strategy, while Parking and Warehouse archetypes could be considered for the “Shallow Retrofit and Reuse” strategy. Most Single-family archetypes are suitable for a deep energy retrofit or can be replaced, while the majority of Multi-family buildings would need a shallow energy retrofit or a replacement. Figures 4.22 to 4.24 present a closer view of the different strategies proposed for each archetype.

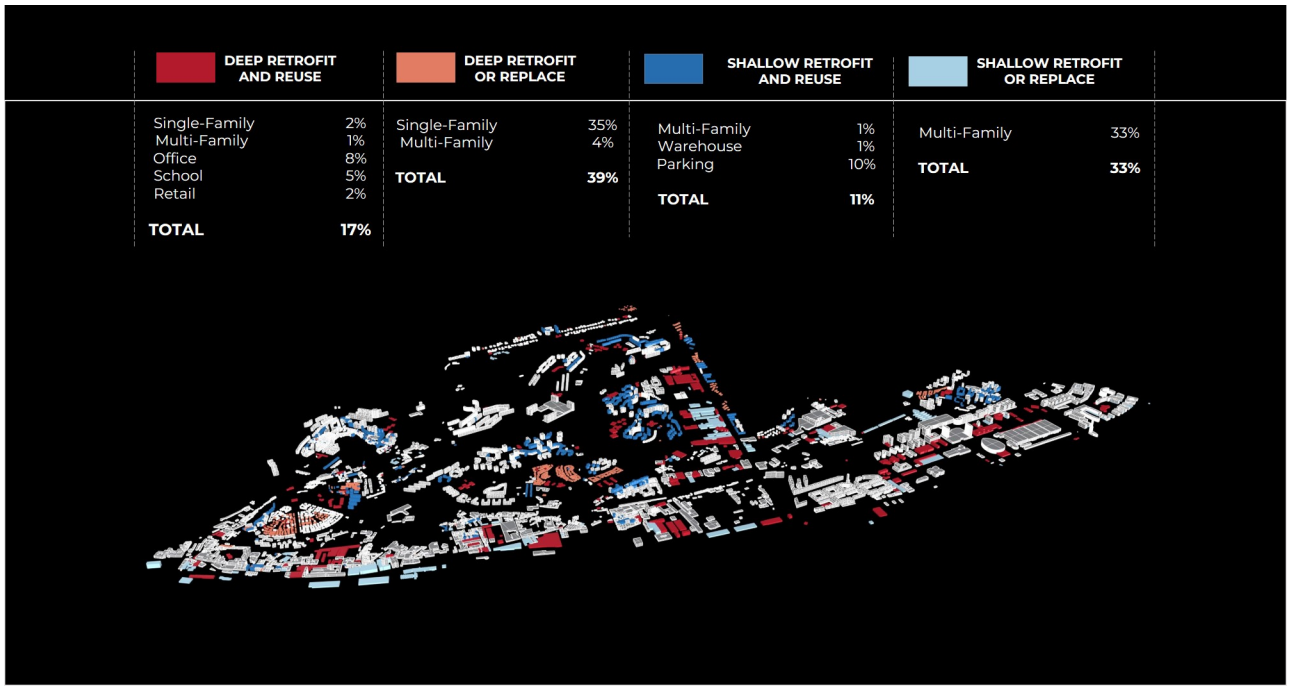

Figure 4.21: Spatial Distribution of Buildings Based on Stock-level Recommendations.

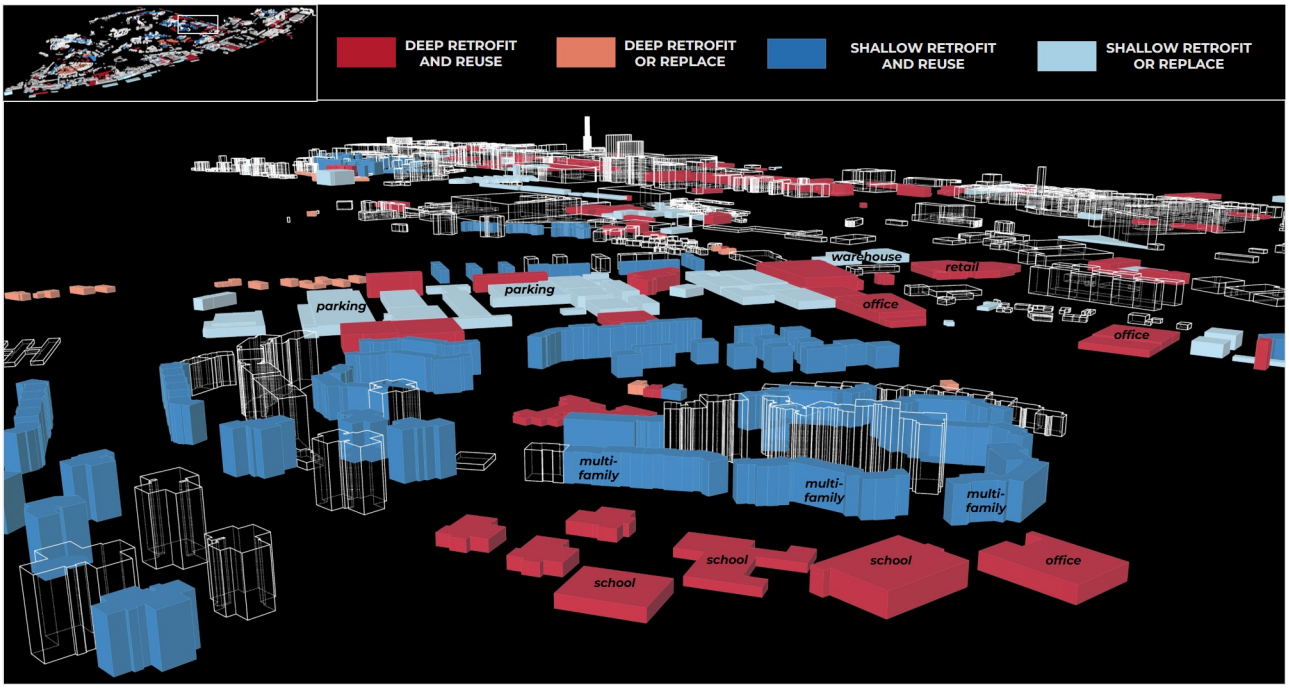

Figure 4.22: Rendering of Recommendations for Different Building Archetypes.

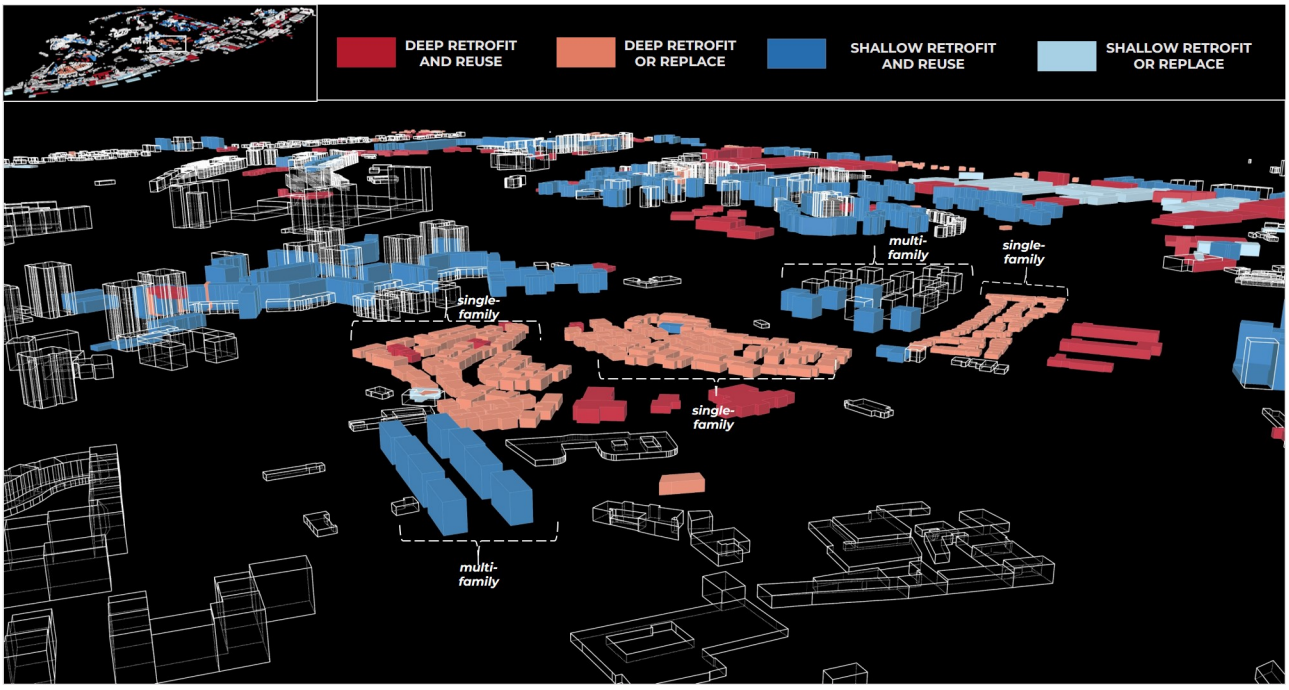

Figure 4.23: Comparison of Recommendations for Multi-family and Single-family (1/2).

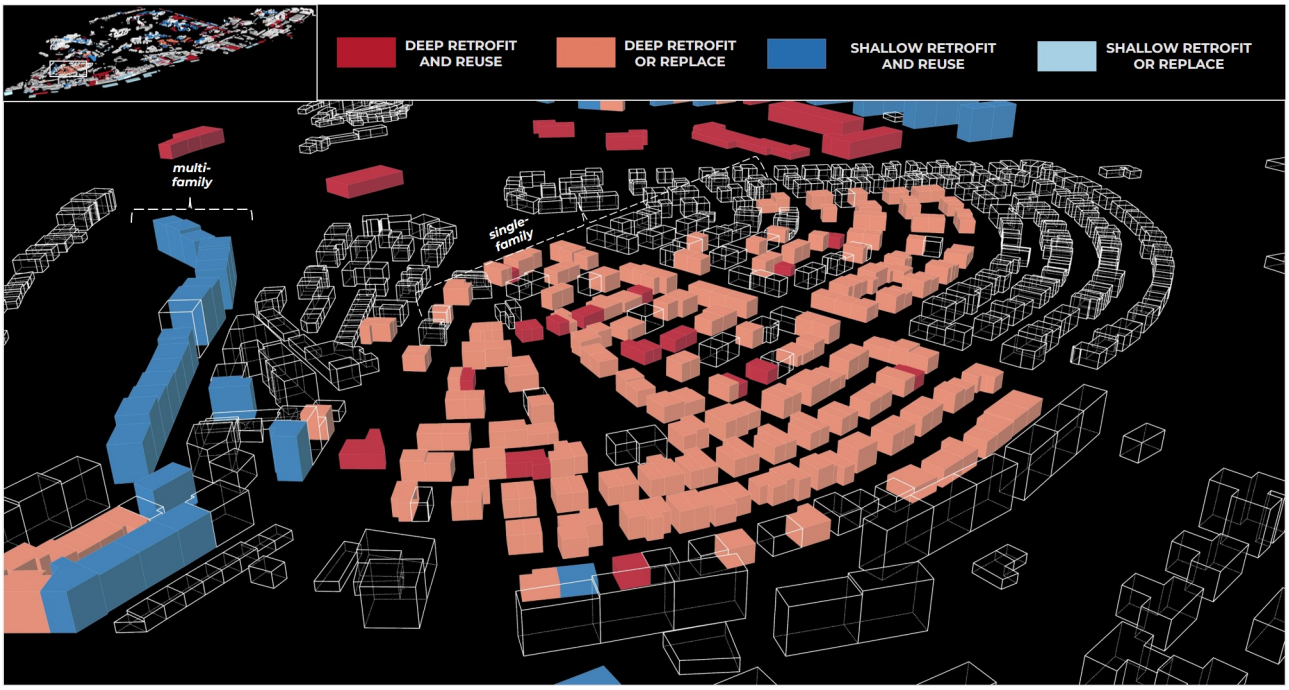

Figure 4.24: Comparison of Recommendations for Multi-family and Single-family (2/2).

Chapter 5

Conclusion

5.1 Summary of Contributions

The work presented in this thesis demonstrates the development and application of a new physics-based and data-driven model for rapidly predicting the total embodied carbon of a building's structural system with a few key inputs in early-stage design. A large synthetic dataset was generated from a parametric model of a reinforced concrete multi-story building. The exploratory data analysis provided valuable insights into understanding the parametric model design space and anticipating some behaviors of the Neural Network model. After training, validating, and testing the surrogate model, it is capable of automatically estimating the volumetric material quantities of the entire structural system without requiring an elaborate FEA. The model performs reasonably well and can be directly applied to the rapid early-stage estimation of structural material quantities for embodied carbon assessment in urban modeling.

After deploying the surrogate model into the urban modeling tool, UMI, it was possible to perform a sensitivity analysis at the individual-building scale and rapidly estimate and map the spatial distribution of embodied and operational carbon for an entire neighborhood in Lisbon as if it were built again today. The benchmarks obtained can be considered as baselines when evaluating the environmental impact of new construction. Moreover, comparing these benchmarks with existing studies demonstrated the advantage of specific stock-level analysis for more accuracy. The integrated assessment conducted in the case study provides an opportunity to evaluate the tradeoffs between embodied and operational carbon at the urban level and guide planning and policy decision-making through stock-level recommendations on retrofitting strategies or new construction.

Therefore, the ultimate contribution of this work is to demonstrate that urban modeling of embodied carbon is feasible using the methodology proposed and that greater accuracy can be achieved by integrating physics-based estimates of structural material quantities within building archetypes.

5.2 Potential Impact

This work is grounded in well-established structural engineering calculations and contributes by creating an algorithmically-generated BIM with high fidelity given limited inputs. The methodology used addresses the current gap for estimating the embodied carbon of the structural system in early-stage design when there is a lack of knowledge on design variables. Therefore, this might lead to a significant positive impact on the ability of architects and engineers to effectively reduce the carbon footprint of a design in the early stages.

Indeed, the analysis of the synthetic database collected from the parametric model pinpoints the three most impactful design variables of multi-storey buildings to be the primary span, concrete strength and live load. Moreover, the sensitivity study results successfully demonstrate that the physics-based structural quantities estimates from the surrogate model allow more nuanced embodied carbon assessments by fine-tuning the structural parameters of pre-defined building archetypes.

Currently, very few urban modeling tools include an embodied model, which contains the information that structural engineers typically use in the design process: the structural loads, mechanical properties, and soil conditions. Therefore, this methodology can provide valuable insights when integrated on a large scale within an urban modeling tool such as UMI. For example, the main findings of the Lisbon case study reveal that in all commercial building archetypes, the Structure has a larger contribution to the upfront embodied carbon than the Envelope & Interior, while the reverse is true for residential archetypes. Therefore, the impact of this research provides an opportunity to create local, regional, and even national benchmarks of embodied carbon from available GIS data.

5.3 Limitations and Future Work

Some limitations remain to the implementation of the physics-based and data-driven model in early-stage design and urban modeling.
First, the structural model only considers the gravity system of typical rectangular structural frames. More complex frames, including lateral systems, should be considered in the future as they were proven to be more carbon-intensive.
Second, the most time-intensive part of implementing this process in urban modeling is collecting data for creating complete archetypes, including both operational and embodied models. This requires some knowledge of local construction standards and manually populating archetypes with enough information to perform the urban-scale analysis.

Finally, future work can expand the structural system model for different materials and typologies and validate the outputs with real data. This way, this methodology can be applied across different scales and case studies.

5.4 Concluding Remarks

In this work, a physics-based and data-driven model allows to estimate the structural system's embodied carbon in reinforced concrete building archetypes in early-stage design and on a large scale with increased accuracy and speed.

By quickly mapping embodied and operational carbon with this new method, carbon hotspots, and more accurate benchmarks can be easily identified at the urban level. Indeed, integrating this analysis into urban modeling tools allows a more granular estimation of embodied carbon to gain valuable insights from the existing building stock. Such tools and methodologies can provide users with different ways to leverage this information. Designers, urban planners, and policy-makers can better understand where the most carbon-intensive buildings are located. They can also infer the cause explaining such higher embodied and operational carbon by finding which building system contributes the most.

To conclude, this thesis developed a new methodology to support architects, structural engineers, and urban planners in making better design and planning decisions from the earliest design stages toward the Net Zero Embodied and Operational reduction goal.

Appendix A

Sensitivity Study

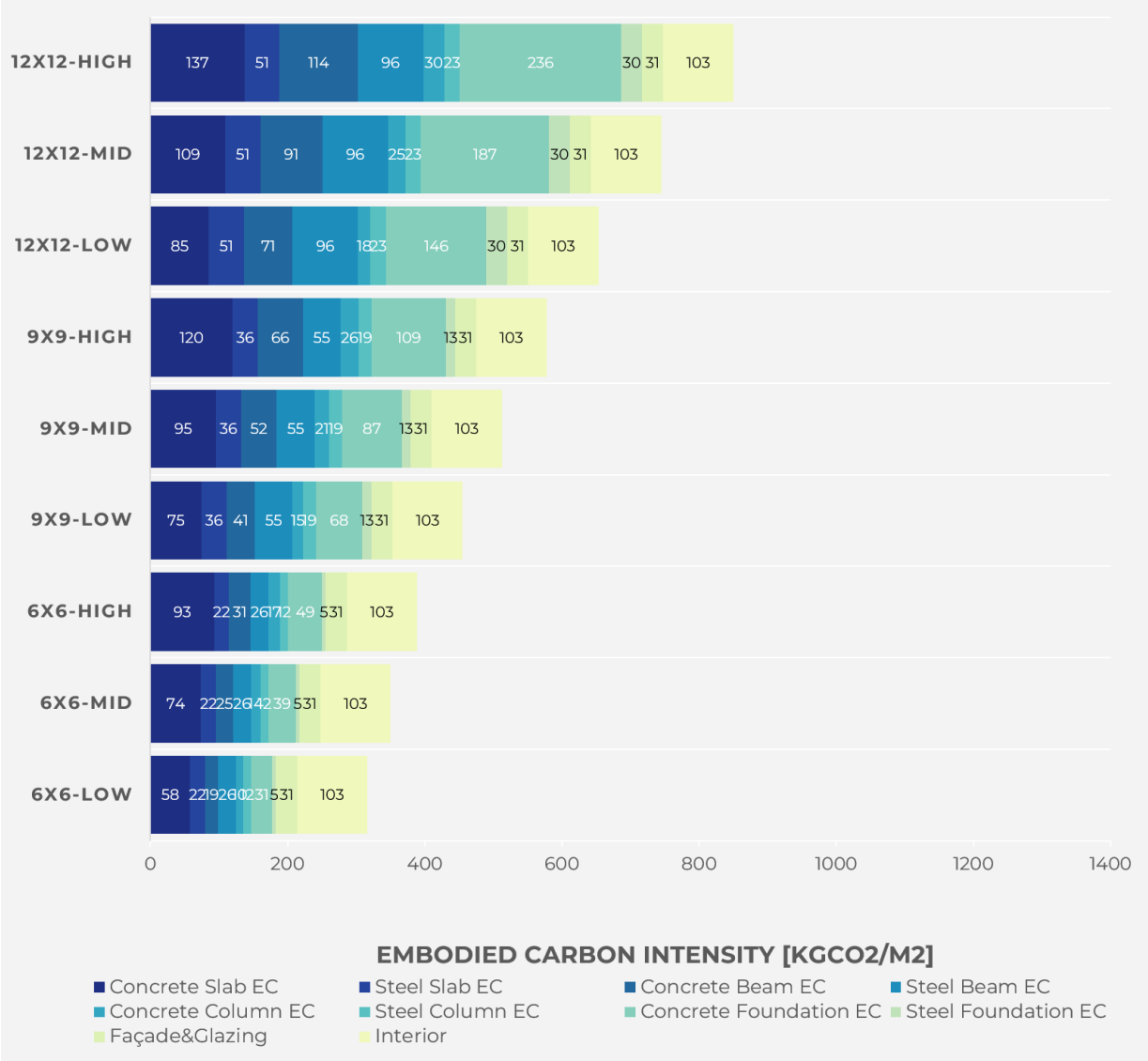

Figure A.1: Multi-Family Sensitivity Study Results.

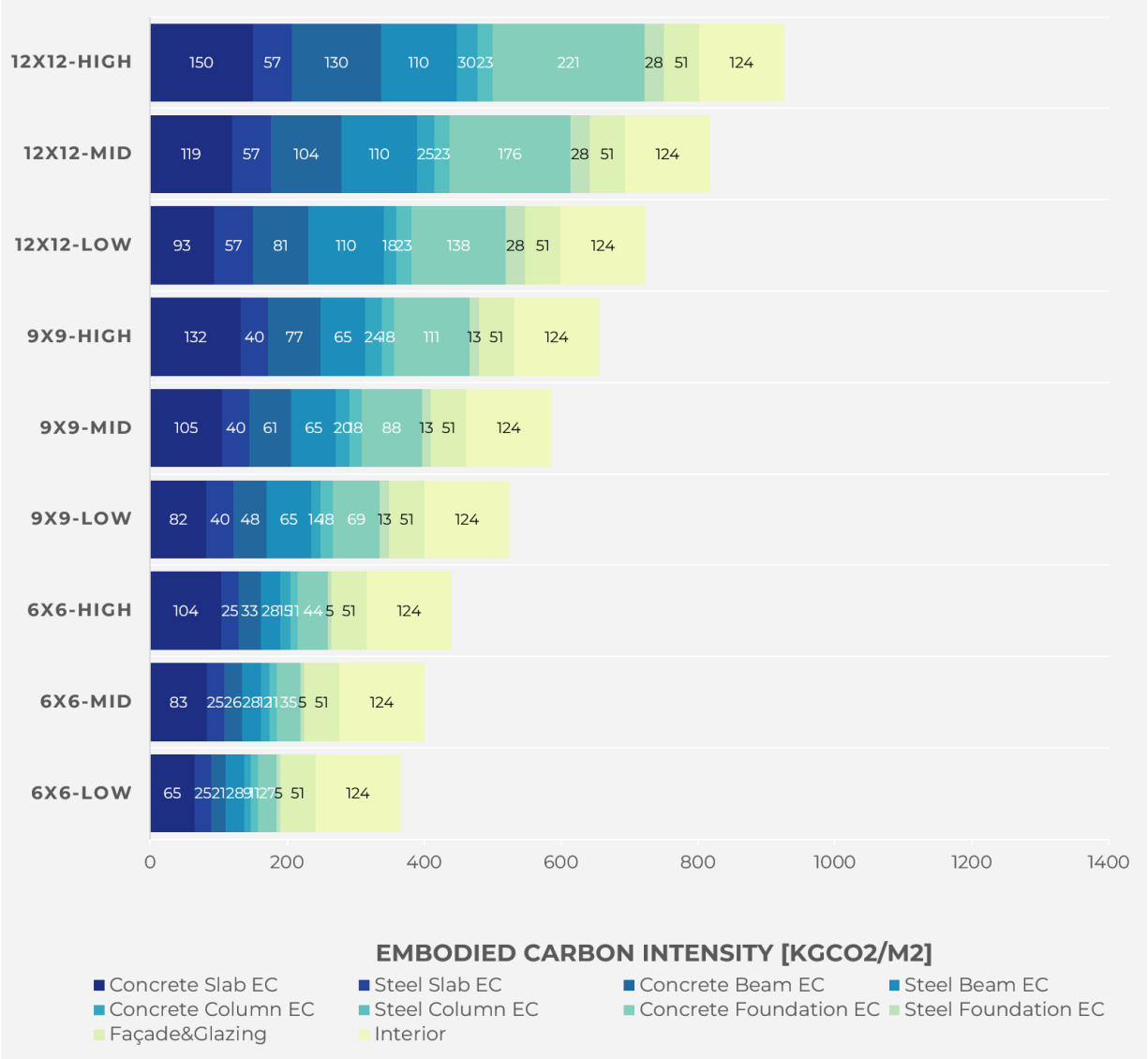

Figure A.2: Single-Family Sensitivity Study Results.

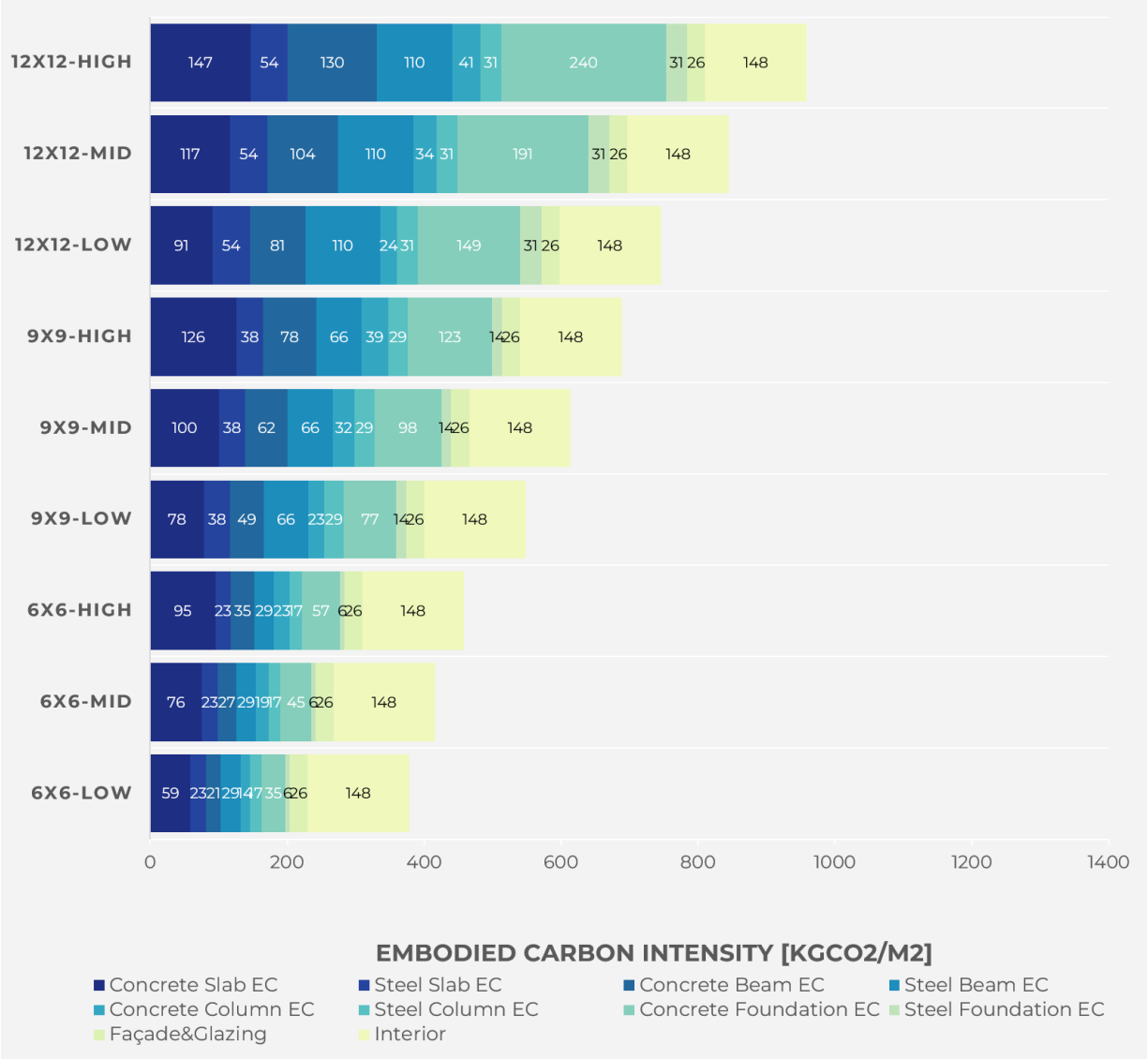

Figure A.3: Office Sensitivity Study Results.

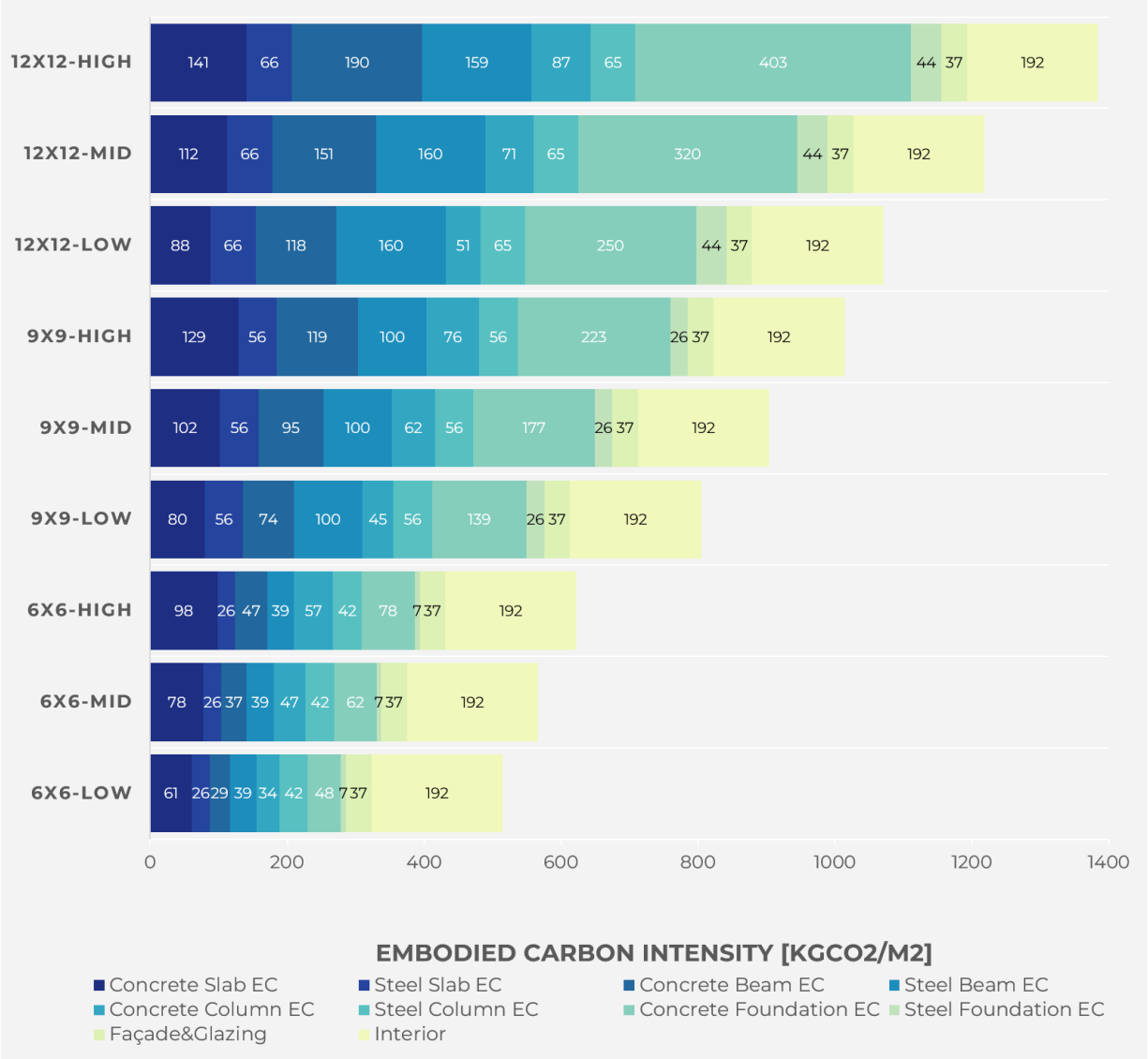

Figure A.4: Warehouse Sensitivity Study Results.

References

Abbasabadi, N., & Ashayeri, M. (2019). Urban energy use modeling methods and tools_ A review and an outlook. Retrieved 2022-03-09, from https://www.sciencedirect.com/science/article/pii/S0360132319304809 doi: 10.1016/j.buildenv.2019.106270

Ali, U., Shamsi, M. H., Hoare, C., Mangina, E., & O'Donnell, J. (2021, September). Review of urban building energy modeling (UBEM) approaches, methods and tools using qualitative and quantitative analysis. *Energy and Buildings*, *246*, 111073. Retrieved 2023-02-26, from https://www.sciencedirect.com/science/article/pii/S0378778821003571 doi: 10.1016/j.enbuild.2021.111073

Ang, Y. Q., Berzolla, Z. M., Letellier-Duchesne, S., & Reinhart, C. F. (2023, April). Carbon reduction technology pathways for existing buildings in eight cities. *Nature Communications*, *14*(1), 1689. Retrieved 2023-04-13, from https://www.nature.com/articles/s41467-023-37131-6 doi: 10.1038/s41467-023-37131-6

Architecture2030. (2023). *Why The Building Sector? – Architecture 2030.* Retrieved 2023-04-19, from https://architecture2030.org/why-the-building-sector/

Bowick, M., O'Connor, J., & Meil, J. (2014). *Athena Guide to Whole-Building LCA in Green Building Programs* (Tech. Rep.).

Cerezo Davila, C. (2017). *Building archetype calibration for effective urban building energy modeling* (Thesis, Massachusetts Institute of Technology). Retrieved 2022-06-15, from https://dspace.mit.edu/handle/1721.1/111487

D'Amico, B., & Pomponi, F. (2020, September). On mass quantities of gravity frames in building structures. *Journal of Building Engineering*, *31*, 101426. Retrieved 2022-05-16, from https://linkinghub.elsevier.com/retrieve/pii/S2352710219315050 doi: 10.1016/j.jobe.2020.101426

De Wolf, C., Pomponi, F., & Moncaster, A. (2017, April). Measuring embodied carbon dioxide equivalent of buildings: A review and critique of current industry practice. *Energy and Buildings*, *140*, 68–80. Retrieved 2021-09-25, from https://www.sciencedirect.com/science/article/pii/S0378778817302815 doi: 10.1016/j.enbuild.2017.01.075

De Wolf, C., Yang, F., Cox, D., Charlson, A., Hattan, A. S., & Ochsendorf, J. (2015, August). Material quantities and embodied carbon dioxide in structures. *Proceedings of the Institution of Civil Engineers - Engineering Sustainability*, *169*(4), 150–161. Retrieved 2021-10-30, from http://www.icevirtuallibrary.com/doi/10.1680/ensu.15.00033 doi: 10.1680/ensu.15.00033

Dunant, C. F., Drewniok, M. P., Orr, J. J., & Allwood, J. M. (2021, October). Good early stage design decisions can halve embodied CO2 and lower structural frames' cost. *Structures*, *33*, 343–354. Retrieved 2022-08-04, from https://linkinghub.elsevier.com/retrieve/pii/S2352012421003325 doi: 10.1016/j.istruc.2021.04.033

EPA. (2022). *U.S. Energy Information Administration - EIA - Independent Statistics and Analysis - Carbon Dioxide Emissions Coefficients.* Retrieved 2023-04-20, from https://www.eia.gov/environment/emissions/co2_vol_mass.php

Fang, D., Brown, N. C., De Wolf, C., & Mueller, C. (2023). Reducing embodied carbon in structural systems: a review of early-stage design strategies (under preparation). *Journal of Building Engineering*.

Feickert, K. A. (2022). *Thin shell foundations: Embodied carbon reduction through materially efficient geometry* (Thesis, Massachusetts Institute of Technology). Retrieved 2023-04-17, from https://dspace.mit.edu/handle/1721.1/144920

Gauch, H. L., Dunant, C. F., Hawkins, W., & Cabrera Serrenho, A. (2023, March). What really matters in multi-storey building design? A simultaneous sensitivity study of embodied carbon, construction cost, and operational energy. *Applied Energy*, *333*, 120585. Retrieved 2023-01-16, from https://www.sciencedirect.com/science/article/pii/S0306261922018426 doi: 10.1016/j.apenergy.2022.120585

Hens, I., Solnosky, R., & Brown, N. C. (2021, August). Design space exploration for comparing embodied carbon in tall timber structural systems. *Energy and Buildings*, *244*, 110983. Retrieved 2021-06-21, from https://www.sciencedirect.com/science/article/pii/S037877882100267X doi: 10.1016/j.enbuild.2021.110983

International Energy Agency. (2021). *Portugal 2021 Energy Policy Review*. OECD. Retrieved 2023-04-28, from https://www.oecd-ilibrary.org/energy/portugal-2021-energy-policy-review_3b485e25-en doi: 10.1787/3b485e25-en

Ismail, M. A., & Mueller, C. T. (2021, November). Minimizing embodied energy of reinforced concrete floor systems in developing countries through shape optimization. *Engineering Structures*, *246*, 112955. Retrieved 2021-08-26, from https://www.sciencedirect.com/science/article/pii/S0141029621010993 doi: 10.1016/j.engstruct.2021.112955

Kaethner, S. C., & Burridge, J. A. (2012). Embodied CO2 of structural frames.

Kral, K. (2021, January). AutoFrame: A Novel Procedure to Auto-Convert Architectural Massing Models into Structural Simulation Models to Streamline Embodied- and

Operational-Carbon Assessment and Daylight Evaluation in Early Design. *Technology|Architecture + Design*, *5*(1), 59–72. Retrieved 2022-01-15, from https://doi.org/10.1080/24751448.2021.1863674 doi: 10.1080/24751448.2021.1863674

Kuittinen, M., Organschi, A., & Ruff, A. (2023). Carbon : a field manual for building designers. Retrieved 2023-02-10, from https://onlinelibrary.wiley.com/doi/epub/10.1002/9781119720867 (ISBN: 9781119720867)

Marsh, R., Nygaard Rasmussen, F., & Birgisdottir, H. (2018). Embodied Carbon Tools for Architects and Clients Early in the Design Process. In F. Pomponi, C. De Wolf, & A. Moncaster (Eds.), *Embodied Carbon in Buildings: Measurement, Management, and Mitigation* (pp. 167–190). Retrieved from https://doi.org/10.1007/978-3-319-72796-7_8 doi: 10.1007/978-3-319-72796-7_8

Monteiro, C. S., Pina, A., Cerezo, C., Reinhart, C., & Ferrão, P. (2017, March). The Use of Multi-detail Building Archetypes in Urban Energy Modelling. *Energy Procedia*, *111*, 817–825. Retrieved 2022-06-14, from https://www.sciencedirect.com/science/article/pii/S1876610217302771 doi: 10.1016/j.egypro.2017.03.244

Nicholson, S., & Heath, G. (2021). NREL Life Cycle Greenhouse Gas Emissions from Electricity Generation. Retrieved from https://www.nrel.gov/docs/fy21osti/80580.pdf

OurWorldinData. (2023). *Our World in Data.* Retrieved 2022-08-17, from https://ourworldindata.org

Pomponi, F., Anguita, M. L., Lange, M., D'Amico, B., & Hart, E. (2021). Enhancing the Practicality of Tools to Estimate the Whole Life Embodied Carbon of Building Structures via Machine Learning Models. *Frontiers in Built Environment*, *7*. Retrieved 2023-02-25, from https://www.frontiersin.org/articles/10.3389/fbuil.2021.745598

Pomponi, F., & Moncaster, A. (2018, January). Scrutinising embodied carbon in buildings: The next performance gap made manifest. *Renewable and Sustainable Energy Reviews*, *81*, 2431–2442. Retrieved 2021-09-25, from https://www.sciencedirect.com/science/article/pii/S136403211730998X doi: 10.1016/j.rser.2017.06.049

Reyna, J., Wilson, E., Parker, A., Satre-Meloy, A., Egerter, A., Bianchi, C., . . . Rothgeb, S. (2022). U.S. Building Stock Characterization Study: A National Typology for Decarbonizing U.S. Buildings. *Renewable Energy*.

Röck, M., Sørensen, A., Tozan, B., Steinmann, J., Horup, L. H., Le Den, X., & Birgisdottir, H. (2022, March). *Towards embodied carbon benchmarks for buildings in Europe - #2 Setting the baseline: A bottom-up approach* (Tech. Rep.). Retrieved 2022-07-21, from https://zenodo.org/record/5895051

Simonen, K., Rodriguez, B. X., & De Wolf, C. (2017, November). Benchmarking the Embodied Carbon of Buildings. *Technology|Architecture + Design*, *1*(2), 208–218. Retrieved 2021-09-25, from https://doi.org/10.1080/24751448.2017.1354623 doi: 10.1080/24751448.2017.1354623

Stephan, A., & Athanassiadis, A. (2017, March). Quantifying and mapping embodied environmental requirements of urban building stocks. *Building and Environment*, *114*, 187–202. Retrieved 2023-04-11, from https://www.sciencedirect.com/science/article/pii/S0360132316304747 doi: 10.1016/j.buildenv.2016.11.043

Tseranidis, S., Brown, N. C., & Mueller, C. T. (2016, December). Data-driven approximation algorithms for rapid performance evaluation and optimization of civil structures. *Automation in Construction*, *72*, 279–293. Retrieved 2022-05-06, from https://www.sciencedirect.com/science/article/pii/S0926580516300243 doi: 10.1016/j.autcon.2016.02.002

UMI. (2023). *Urban Modeling Interface · GitHub.* Retrieved 2023-04-29, from https://github.com/UrbanModelingInterface

Victoria, M. F., & Perera, S. (2018, June). Parametric embodied carbon prediction model for early stage estimating. *Energy and Buildings*, *168*, 106–119. Retrieved 2023-01-24, from https://www.sciencedirect.com/science/article/pii/S0378778817321813 doi: 10.1016/j.enbuild.2018.02.044

Weber, R., Mueller, C., & Reinhart, C. (2021, October). *Building for Zero, The Grand Challenge of Architecture without Carbon* [SSRN Scholarly Paper]. Rochester, NY. Retrieved 2023-02-14, from https://papers.ssrn.com/abstract=3939009 doi: 10.2139/ssrn.3939009

Weber, R. E., Mueller, C., & Reinhart, C. (2021, August). Generative Structural Design for Embodied Carbon Estimation. In *Proceedings of the IASS Annual Symposium 2020/21 and the 7th International Conference on Spatial Structures.* Guilford, UK.

Xavier, V., Couto, R., Monteiro, R., Castro, J. M., & Bento, R. (2022, May). Detailed Structural Characterization of Existing RC Buildings for Seismic Exposure Modelling of the Lisbon Area. *Buildings*, *12*(5), 642. Retrieved 2023-03-08, from https://www.mdpi.com/2075-5309/12/5/642 doi: 10.3390/buildings12050642